Effects of organic coating on the nitrate formation by suppressing the N_2O_5 heterogeneous hydrolysis: A case study during wintertime in Beijing-Tianjin-Hebei (BTH)

Lang Liu[1,4], Jiarui Wu[1], Suixin Liu[1], Xia Li[1], Jiamao Zhou[1], Tian Feng[1], Yang Qian[3], Junji Cao[1,2], Xuexi Tie[1], Guohui Li[1,2*]

[1]Key Lab of Aerosol Chemistry and Physics, SKLLQG, Institute of Earth Environment, Chinese Academy of Sciences, Xi'an, China
[2]CAS Center for Excellence in Quaternary Science and Global Change, Xi'an, China
[3]State Key Laboratory of Environmental Criteria and Risk Assessment & Environmental Standards Institute, Chinese Research Academy of Environmental Sciences, Beijing, China
[4]University of Chinese Academy of Sciences, Beijing, China

Correspondence to: Guohui Li (ligh@ieecas.cn)

Abstract: Although stringent emission mitigation strategies have been carried out since 2013 in Beijing-Tianjin-Hebei (BTH), China, heavy haze with high levels of fine particulate matter ($PM_{2.5}$) still frequently engulfs the region during wintertime and the nitrate contribution to $PM_{2.5}$ mass has progressively increased. The N_2O_5 heterogeneous hydrolysis is the most important pathway of the nitrate formation at nighttime. In the present study, the WRF-Chem model is applied to simulate a heavy haze episode from 10 to 27 February 2014 in BTH to evaluate contributions of the N_2O_5 heterogeneous hydrolysis to nitrate formation and effects of organic coating. The model generally performs reasonably well in simulating meteorological parameters, air pollutants and aerosol species against observations in BTH. The N_2O_5 heterogeneous hydrolysis with all the secondary organic aerosol assumed to be involved in coating considerably improves the nitrate simulations compared to the measurements in Beijing. On average, organic coating decreases nitrate concentrations by 8.4% in BTH during the episode, and the N_2O_5 heterogeneous hydrolysis with organic coating contributes about 30.1% of nitrate concentrations. Additionally, the reaction also plays a considerable role in the heavy haze formation, with a $PM_{2.5}$ contribution of about 11.6% in BTH. Sensitivity studies also reveal that future studies need to be conducted to predict the organic aerosol hygroscopicity for accurately representing the organic coating effect on the N_2O_5 heterogeneous hydrolysis.

1 Introduction

Within recent decades, China has been suffering from pervasive and persistent haze pollution caused by elevated levels of fine particulate matters ($PM_{2.5}$), particularly in Beijing-Tianjin-Hebei (BTH) (Guo et al., 2014; Gao et al., 2016; Wang et al., 2016). Numerous studies have revealed that the inorganic aerosols, including nitrate, sulfate and ammonium, are the most abundant component of $PM_{2.5}$ during haze pollution episodes in BTH, and that the evolution of the haze pollution is characterized by the formation of substantial amounts of sulfate and nitrate (Sun et al., 2013; Zhang et al., 2013; Zhao et al., 2013; Sun et al., 2015). Since 2013, several aggressive emission control strategies have been implemented in China, including desulfurization and dedusting for coal combustion, vehicle restriction and executing stringent emission standards in the key industries (Tao et al., 2017). However, the control of emissions of nitrate gaseous precursors does not seem to be effective, since many observations have shown that the nitrate aerosol concentration has progressively increased in recent several years (Zhang et al., 2012; Sun et al., 2015; Zhang et al., 2015; Tao et al., 2017).

In the atmosphere, nitrate aerosol is formed via nitrous acid (HNO_3) to balance the inorganic cations in the aerosol phase. HNO_3 is produced through four pathways (Kim et al., 2014): (1) the reaction of OH and NO_2 (main gas phase pathway and usually considered as the daytime pathway because the OH radical is severely limited at night due to lack of O_3 and peroxide photolysis), (2) NO_3 radical reaction with hydrocarbons, (3) aqueous reaction of NO_3 radical to form HNO_3, and (4) NO_3 conversion to N_2O_5 with subsequently heterogeneous chemical conversion to form HNO_3. The last pathway is referred to as the most important pathway during nighttime, since both NO_3 and N_2O_5 are photolytically liable, or even under heavy haze situation with weak sunlight and high relative humidity (RH) (Brown et al., 2016).

The heterogeneous hydrolysis of N_2O_5 on the surface of deliquescent aerosols to form HNO_3 is quantified by the reaction probability ($\gamma_{N_2O_5}$) (Bertram and Thornton, 2009; Chen et al., 2018; Davis et al., 2008; Riemer et al., 2003). $\gamma_{N_2O_5}$ has been measured by previous laboratory experiments, dependent on particulate chemical composition, RH, temperature, aerosol surface area and water content (Chang et al., 2011), and in the order of 10^{-2} (Zheng et al., 2015). In modeling studies, various parameterizations of $\gamma_{N_2O_5}$ are used to simulate the nitrate formation. Dentener and Crutzen (1993) have first used 0.1 as the representative $\gamma_{N_2O_5}$ in a three-dimensional global model. Riemer et al. (2003) have developed a $\gamma_{N_2O_5}$ parameterization on the surface of aerosols containing sulfate and nitrate (hereafter referred as to Riemer03), which has widely been used and further improved in air quality models. Davis et al. (2008) have implemented a $\gamma_{N_2O_5}$ parameterization on the surface of particles containing sulfate, nitrate, ammonium, as a function of RH, temperature and phase state, to improve simulations of N_2O_5 hydrolysis. Bertram and Thornton (2009) have developed a parameterization to consider the influence of chloride salts on $\gamma_{N_2O_5}$ as a function of RH.

The coating of particles by organic materials has been reported to inhibit N_2O_5 uptake (Anttila et al., 2006), and suggested as a possible explanation for field observations of suppressed N_2O_5 uptake (Brown et al., 2006). Evans and Jacob (2005) have incorporated a $\gamma_{N_2O_5}$ parameterization on surfaces of sulfate particles as a function of RH and temperature into the GEOS-CHEM model, including the effects of dust, sea salt, sulfate, elemental carbon and organic carbon but ignoring the nitrogen-containing species. Riemer et al. (2009) have developed a N_2O_5 uptake parameterization (Riemer09) based on the laboratory results of Anttila et al. (2006), which combines the nitrogen-containing and organic effects on N_2O_5 hydrolysis. The parameterization has been used to estimate the maximum effect of organic coating by assuming that all available secondary organic compounds (SOC) contribute to the coating in a 3-D model. The results show that SOC could suppress N_2O_5 uptake significantly,

reducing particulate nitrate concentrations by up to 90%. Lowe et al. (2015) have further combined the organic coating and chloride salts effects on $\gamma_{N_2O_5}$ in the WRF-Chem model. Most recently, Chen et al. (2018) have developed a new $\gamma_{N_2O_5}$ parameterization with respect to RH, temperature, and aerosol composition, showing that organic coating effect on $\gamma_{N_2O_5}$ is not as important as expected over western and central Europe. However, there is still a lack of modeling studies focused on the effect of organic coating on $\gamma_{N_2O_5}$ and particulate nitrate formation in China. Wang et al. (2017) have evaluated the potential particulate nitrate formation through the N_2O_5 hydrolysis reaction without considering the organic coating effect during a haze pollution episode in Beijing, and found that the observed nitrate concentration (20.6 μg m^{-3} on average) is lower than the assessment (57.0 μg m^{-3} on average). Considering the high organic aerosol concentration and increasing trend of particulate nitrate during haze days in BTH, it is imperative to assess the effect of organic coating on N_2O_5 hydrolysis and its consequent contribution to the nitrate formation.

In the present study, based on Riemer09 parameterization, the contribution of the organic coating effect on N_2O_5 hydrolysis to the nitrate formation is investigated using the WRF-Chem model. The model configuration and methodology are described in Section 2. Results and sensitivity studies are presented in Section 3. Discussion and summary are given in section 4.

2 Model and Methodology

2.1 WRF-Chem model and configuration

A modified version of the WRF-Chem model (Grell et al., 2005) is used in this study, which is developed by Li et al. (2010; 2011a; 2011b; 2012) at the Molina Center for Energy and the Environment. A new flexible gas phase chemical module has been developed and implemented into the version of the WRF-Chem model, which can be utilized with different

chemical mechanisms, including CBIV, RADM2, and SAPRC. The gas-phase chemistry is solved by an Eulerian backward Gauss-Seidel iterative technique with a number of iterations, inherited from NCAR-HANK (Hess et al., 2000). In the study, the SAPRC99 chemical mechanism is used based on the available emission inventory. For the aerosol simulations, the CMAQ/models3 aerosol module (AERO5) developed by US EPA has incorporated into the model (Binkowski and Roselle, 2003). Briefly, the wet deposition uses the method in the CMAQ module and the dry deposition of chemical species is parameterized following Wesely (1989). The photolysis rates are calculated using the Fast Tropospheric Ultraviolet and Visible Radiation Model (FTUV; Tie et al., 2003; Li et al., 2005), with the aerosol and cloud effects on the photochemistry (Li et al., 2011a).

ISORROPIA (version 1.7) is used to predict the thermodynamic equilibrium between the ammonia-sulfate-nitrate-chloride-water aerosols and their gas phase precursors of H_2SO_4-HNO_3-NH_3-HCl-water vapor. It is worth noting that the most recent extension of ISORROPIA, known as ISORROPIA II, has incorporated a larger number aerosol species (Ca, Mn, K salts) and is designed to be a superset of ISORROPIA (Fountoukis and Nenes, 2007). Considering that crustal species are not considered in the study, ISORROPIA (version 1.7) is still used to calculate inorganic components and ISORROPIA II is imperative to be incorporated into the WRF-Chem model in future studies. In addition, a parameterization of sulfate heterogeneous formation involving aerosol liquid water (ALW) has been developed and implemented into the model, which has successfully reproduced the observed rapid sulfate formation during haze days (Li et al., 2017). The sulfate heterogeneous formation from SO_2 is parameterized as a first order irreversible uptake by ALW surfaces, with a reactive uptake coefficient of 0.5×10^{-4} assuming that there is enough alkalinity to maintain the high iron-catalyzed reaction rate.

The OA module is based on the VBS approach with aging and detailed information can

be found in Li et al. (2011b). The POA components from traffic-related combustion and biomass burning are represented by nine surrogate species with saturation concentrations (C*) ranging from 10^{-2} to 10^{6} μg m^{-3} at room temperature (Shrivastava et al., 2008), and assumed to be semi-volatile and photochemically reactive (Robinson et al., 2007). The SOA formation from each anthropogenic or biogenic precursor is calculated using four semi-volatile VOCs with effective saturation concentrations of 1, 10, 100, and 1000 μg m^{-3} at 298 K. The SOA formation via the heterogeneous reaction of glyoxal and methylglyoxal is parameterized as a first-order irreversible uptake by aerosol particles with an uptake coefficient of 3.7×10^{-3} (Liggio et al., 2005; Zhao et al., 2006; Volkamer et al., 2007). The OA module has reasonably reproduced the POA and SOA concentration against measurements, and detailed model performance can be found in Li et al. (2011b), Feng et al. (2016), and Xing et al. (2019).

The anthropogenic emission inventory with a horizontal resolution of 6 km is developed by Zhang et al. (2009), with the base year of 2013, including industry, transportation, power plant, residential and agriculture sources. The Model of Emissions of Gases and Aerosols from Nature (MEGAN) is used to calculate the biogenic emissions online (Guenther et al., 2006).

A heavy haze episode from 10 to 27 February 2014 in BTH is simulated in association with the field observation of air pollutants and secondary inorganic aerosols. Detailed model configuration can be found in Table 1 and the simulation domain is presented in Figure 1.

2.2 Parameterization of the heterogeneous hydrolysis of N_2O_5

The reaction of N_2O_5 heterogeneous hydrolysis on the surface of deliquescent aerosols to form HNO_3 can be represented as:

$$N_2O_5 + H_2O \rightarrow 2 \cdot HNO_3 \quad \text{(Eq. 1)}$$

This reaction is usually implemented into air quality transport models as a first order loss:

$$\frac{\partial[N_2O_5]}{\partial t} = -k_{N_2O_5} \cdot [N_2O_5] \quad \text{(Eq. 2)}$$

$[N_2O_5]$ represents the N_2O_5 concentration in the atmosphere. The loss rate constant, $k_{N_2O_5}$, is parameterized in the following way:

$$k_{N_2O_5} = \frac{1}{4} \cdot c_{N_2O_5} \cdot S \cdot \gamma_{N_2O_5} \quad \text{(Eq. 3)}$$

Where $c_{N_2O_5}$ is the average molecular velocity of N_2O_5, and S is the available aerosol surface area density.

In this study, the parameterization of $\gamma_{N_2O_5}$ follows Riemer03 and Riemer09. In the parameterization, the primary emission compounds such as element carbon, insoluble organic matter (most part of POA), insoluble inorganic and mineral dust particles are assumed to serve as a nucleus of aerosols. Condensation of soluble chemical components and further water vapor on the surface of the nucleus forms an aqueous layer. The nucleus and the aqueous layer are assumed as unified "core" (aqueous core) in Riemer03 and Riemer09 parameterizations. In Riemer03 parameterization, soluble inorganic components including sulfate and nitrate are taken into consideration for suppressing the N_2O_5 heterogeneous hydrolysis uptake in the aqueous core, and the parameterization of $\gamma_{N_2O_5}$ is defined as:

$$\gamma_{N_2O_5} = f \cdot \gamma_1 + (1 - f) \cdot \gamma_2 \quad \text{(Eq. 4)}$$

with $\gamma_1 = 0.02$ and $\gamma_2 = 0.002$, and f is defined as:

$$f = \frac{m_{SO_4^{2-}}}{m_{SO_4^{2-}} + m_{NO_3^-}} \quad \text{(Eq. 5)}$$

$m_{SO_4^{2-}}$ and $m_{NO_3^-}$ are the aerosol mass concentrations of soluble sulfate and nitrate.

In Riemer09 parameterization, unreactive organic layers are further considered for the suppression of N_2O_5 hydrolysis by covering the aqueous core. Organic layers may be formed by secondary organic aerosols, and such layers may consist of a single layer of molecules (monolayered coatings) or of several molecule layers (multilayered coatings) on the surface of the aqueous core. These organic layers are assumed as organic "coating" (shell) in the Riemer09 parameterization. The resistor scheme to calculate $\gamma_{N_2O_5}$ in Riemer09

parameterization is parameterized as follows:

$$\frac{1}{\gamma_{N_2O_5}} = \frac{1}{\gamma_{N_2O_5,core}} + \frac{1}{\gamma_{N_2O_5,coat}} \quad \text{(Eq. 6)}$$

where $\gamma_{N_2O_5,core}$ is the reaction probability of the aqueous core which is calculated using Eq. 4, and $\gamma_{N_2O_5,coat}$ is the pseudo-reaction probability of the organic coating calculated by the following formulation:

$$\gamma_{N_2O_5,coat} = \frac{4 \cdot R \cdot T \cdot H_{org} \cdot D_{org} \cdot R_c}{c_{N_2O_5} \cdot \ell \cdot R_p} \quad \text{(Eq. 7)}$$

Where R is the universal gas constant, T is temperature, H_{org} is the Henry's law constant for N_2O_5 in the organic coating, and D_{org} is the diffusion coefficient for N_2O_5 in the organic coating. H_{org} and D_{org} depend on the physicochemical properties of the compounds comprising the organic coating. In the Riemer09 scheme, $H_{org} \cdot D_{org}$ is defined as $0.03 \cdot H_{aq} \cdot D_{aq}$. H_{aq} is the Henry's law constant of N_2O_5 for the aqueous phase (H_{aq}= 5000 M atm^{-1}) and D_{aq} is the diffusion coefficient of N_2O_5 in the aqueous phase (D_{aq}= 10^{-9} m^2 s^{-1}). R_p, R_c, and ℓ are the radius of the particle, radius of the inorganic core, and thickness of the coating, respectively. R_p, R_c, and ℓ are calculated as follows:

$$R_p = R_c + \ell \quad \text{(Eq. 8)}$$

$$\ell = R_p \cdot (1 - \beta^{\frac{1}{3}}) \quad \text{(Eq. 9)}$$

$$\beta = \frac{V_{inorg}}{V_{inorg} + V_{org}} \quad \text{(Eq. 10)}$$

Where V_{inorg} and V_{org} are the volume of inorganic and organic materials, respectively.

2.3 Statistical methods for model evaluation

In this study, the mean bias (MB), root mean square error (RMSE), the index of agreement (IOA), mean fractional bias (MFB) and mean fractional error (MFE) are used to evaluate the model performance in simulating air pollutants.

$$\mathrm{MB} = \frac{1}{\mathrm{N}} \sum_{\mathrm{i}=1}^{\mathrm{N}} (\mathrm{P_i} - \mathrm{O_i}) \quad \text{(Eq. 11)}$$

$$\mathrm{RMSE} = \left[\frac{1}{\mathrm{N}}\sum_{\mathrm{i}=1}^{\mathrm{N}}(\mathrm{P_i} - \mathrm{O_i})^2\right]^{\frac{1}{2}} \quad \text{(Eq. 12)}$$

$$\mathrm{IOA} = 1 - \frac{\sum_{\mathrm{i}=1}^{\mathrm{N}}(\mathrm{P_i}-\mathrm{O_i})^2}{\sum_{\mathrm{i}=1}^{\mathrm{N}}(|\mathrm{P_i}-\bar{\mathrm{O}}|+|\mathrm{O_i}-\bar{\mathrm{O}}|)^2} \quad \text{(Eq. 13)}$$

$$\mathrm{MFB} = \frac{1}{\mathrm{N}}\sum_{\mathrm{i}=1}^{\mathrm{N}}\frac{\mathrm{P_i}-\mathrm{O_i}}{(\mathrm{P_i}+\mathrm{O_i})/2} \quad \text{(Eq. 14)}$$

$$\mathrm{MFE} = \frac{1}{\mathrm{N}}\sum_{\mathrm{i}=1}^{\mathrm{N}}\frac{|\mathrm{P_i}-\mathrm{O_i}|}{(\mathrm{P_i}+\mathrm{O_i})/2} \quad \text{(Eq. 15)}$$

Where P_i and O_i are the simulated and observed variables, respectively. N is the total number of the simulations for comparisons, and $\bar{O}$ donates the average of the observation. The IOA ranges from 0 to 1, with 1 showing a perfect agreement of the simulation with the observation.

2.4 Air pollutants observations

Simulations are compared to available meteorological and air pollutants observations to evaluate the model performance. The meteorological parameters including temperature, RH, wind speed and direction are obtained from the website http://www.meteomanz.com. The hourly observations of $PM_{2.5}$, O_3, SO_2, NO_2, and CO concentrations are released by China National Environmental Monitoring Center and can be downloaded from the website http://106.37.208.233:20035.

Additionally, hourly OC and EC concentrations are measured using a thermal/optical reflectance carbon analyzer (OCEC RT-4, Sunset Lab, USA) at Chinese Research Academy of Environmental Sciences (CRAES, 40.04°N, 116.40°E) in Beijing (Wei et al., 2014; Liu et al., 2018). Hourly sulfate, nitrate, ammonium, and other inorganic ions are sampled and analyzed by ion chromatography (URG 9000S, Thermo Fisher Scientific, USA).

The OC/EC ratio approach is used to derive the SOA mass concentrations from EC and OC filter measurements as follows (Strader, 1999; Cao et al., 2004):

$$POC = EC \times \left(\frac{POC}{EC}\right) \quad \text{(Eq. 16)}$$

$$SOC = OC - POC \quad \text{(Eq. 17)}$$

$$SOA = SOC \times \left(\frac{SOA}{SOC}\right) \quad \text{(Eq. 18)}$$

Where POC and SOC are the primary OC and secondary OC, respectively. In the present study, $\frac{POC}{EC}$ and $\frac{SOA}{SOC}$ are assumed to be 2.4 and 1.6, respectively, based on the previous studies (Cao et al., 2007; Aiken et al., 2008; Yu et al., 2009) and detailed information about the approach can be found in Feng et al. (2016). It is worth noting that those assumed $\frac{POC}{EC}$ and $\frac{SOA}{SOC}$ could potentially affect the model-measurement comparisons.

3 Results and discussion

3.1 Synoptic conditions during the wintertime of 2014

Based on the NCEP FNL reanalysis data (https://rda.ucar.edu/datasets/ds083.2), we have initially performed the analysis of synoptic conditions using the wind, temperature, relative humidity, and geopotential height fields at 500hPa and 850hPa averaged from 10 to 27 February 2014 over China, respectively (Figure 2). At 500hPa, flat westerly winds prevail over BTH and its surrounding area, indicating a stagnant atmospheric circulation conditions (Figure 2a). Moreover, the flat isotherm distribution is similar to that of the isobar at 500hpa, showing that there is no obvious exchange of clod and warm air masses, which together with the flat westerly leads to the weak turbulent mixing in the vertical direction and the stable weather condition (Figure 2b). At 850hPa, the southeast coastal areas of China are controlled by the anti-cyclone whose center locates over the South China Sea (Figure 2c). In the eastern China influenced by the anti-cyclone, the weak southerly wind prevails over the BTH and its surrounding regions, providing a favorable condition for stagnant weather conditions and further the formation of air pollution. With the prevailing southerly wind, the warm and humid air flow and the polluted air mass are subject to being transported from south to north,

aggravating the air pollution in BTH. In addition, high relative humidity conditions facilitate the heterogeneous reactions for the secondary aerosol formation (Figure 2d).

3.2 Model performance

In order to quantify effects of the N_2O_5 heterogeneous hydrolysis and organic coating on the nitrate formation, three experiments have been performed in the study. In the base case, Riemer09 parameterization is used to take into consideration the organic coating effect on the N_2O_5 heterogeneous hydrolysis by assuming that all the SOA is involved in coating (hereafter referred to as B-case). In the first sensitivity case, the contribution of N_2O_5 heterogeneous hydrolysis to the nitrate formation is not considered (hereafter referred to as H0-case); In the second sensitivity case, the organic coating effect is not considered in Riemer09 parameterization (hereafter referred to as C0-case). The simulation results in the B-case are compared to observations in BTH.

3.2.1 Meteorological parameters simulations in Beijing

Considering that the meteorological conditions play a crucial role in air pollution simulations, which determine accumulation or dispersion of pollutants, verifications are first performed for the simulations of meteorological fields. Figure 3 presents the temporal profile of the simulated and observed temperature, RH, wind speed, and wind direction averaged over 12 meteorological sites in Beijing from 10 to 27 February 2014. The WRF-Chem model reproduces well the temporal variation of the surface temperature during the whole episode. The MB and RMSE is -0.2 and 1.7°C, and the IOA reaches 0.94, indicating good agreement of the simulations with observations (Table 2). The simulated temporal RH variations are also well consistent with observations, with the MB, RMSE and IOA of 2.6%, 10.9% and 0.89, respectively. In addition, the model reasonably well tracks the temporal variations of the surface wind, with IOAs of 0.73 and 0.66 for the wind speed and direction, respectively.

3.2.2 Air pollutants simulations in BTH

Figure 4 shows the relationship between observed and simulated mass concentrations of $PM_{2.5}$, O_3, SO_2, NO_2, and CO in Beijing, Tianjin, and Hebei from 10 to 27 February 2014. The correlation coefficient (R) of $PM_{2.5}$ mass concentrations between observations and simulations in Beijing, Tianjin, and Hebei is 0.83, 0.80, and 0.90, respectively, indicating a good performance of the WRF-Chem model in simulating the $PM_{2.5}$ concentration in BTH. The correlation of O_3 and NO_2 mass concentrations between observations and simulations is not as good as that of $PM_{2.5}$ concentrations in BTH, with the R between 0.6 and 0.8. Apparently, the R of SO_2 simulations with observations show that the WRF-Chem model still has difficulties in well simulating SO_2 concentrations in BTH, particularly in Hebei. Except uncertainties from SO_2 emissions, such as source intensities and distributions, diurnal profiles, et al., the bias of simulated wind fields also substantially influences the SO_2 simulation (Bei et al., 2017). Particularly, SO_2 is principally emitted by the point source, including the power plants and agglomerated industrial zones, so the SO_2 simulations is more sensitive to the wind field simulation uncertainties. In terms of R, the SO_2 simulations in Beijing and Tianjin is better than those in Hebei, indicating that the SO_2 emissions in Beijing and Tianjin are generally determined by area sources, i.e., the residential living, but the point source dominates the SO_2 concentration in Hebei. Considering the long-life time of CO in the atmosphere, the CO simulation is decided by its emission and the meteorological fields. The R of CO simulations with observations in BTH ranges from around 0.6 to 0.7, showing that the CO emissions used in the study and simulated meteorological fields are generally reasonable.

Figure 5 presents the diurnal profiles of simulated and observed $PM_{2.5}$, O_3, NO_2, SO_2, and CO mass concentrations averaged over all ambient monitoring stations in BTH during the simulated episode. The WRF-Chem model well reproduces the diurnal variations of the $PM_{2.5}$ mass concentrations against observations in BTH. The MB and RMSE is -6.3 and

309 27.6μg m^{-3}, respectively, and the IOA is 0.96. The model generally well replicates the haze
310 developing stage, but fails to capture the observed spikes of $PM_{2.5}$ mass concentrations,
311 which might be caused by the uncertainty of the simulated meteorological fields or irregular
312 air pollutants emissions (Bei et al., 2017). The simulated O_3 diurnal variations are in good
313 agreement with observations, with the MB and IOA of 1.4 μg m^{-3} and 0.91, respectively. The
314 model tracks well the observed diurnal variations of NO_2 mass concentrations with an IOA of
315 0.92, but it slightly overestimates NO_2 concentrations compared to observations with a MB of
316 6.6 μg m^{-3}. However, during nighttime, the model overestimation is considerable, which is
317 perhaps due to the model biases in modeling nighttime PBL. Although the model reasonably
318 yields the variation trend of the observed SO_2 concentration, with an IOA of 0.85, the
319 dispersion of the simulated SO_2 concentration is rather large, with a RMSE of 27.8 μg m^{-3}. In
320 addition, the model overestimates the SO_2 concentration compared to observations, and the
321 MB is 7.6 μg m^{-3}, which might be mainly caused by the emission inventory that has
322 undergone noticeable changes since implementation of emission control strategies in 2013 in
323 BTH. The model performs well in simulating CO diurnal variations against observations,
324 with the MB and IOA of 0.2 μg m^{-3} and 0.90, respectively.

325 Figure 6 presents the distributions of simulated and observed near-surface mass
326 concentrations of $PM_{2.5}$, O_3, NO_2, and SO_2 along with the predicted wind fields averaged
327 during the episode. Generally, the simulated wind in BTH is weak during the episode and the
328 southerly wind prevails, well corresponding to the synoptic situation at 850hPa and 500hPa,
329 which is favorable for the accumulation of air pollutants. The observed $PM_{2.5}$ concentrations
330 are more than 115 μg m^{-3} on average, showing that BTH suffers from heavy haze pollution
331 (Figure 6a). The model generally well reproduces the spatial distribution of $PM_{2.5}$
332 concentrations against observations, with the $PM_{2.5}$ concentration exceeding 150 μg m^{-3} in
333 the plain area of BTH. The simulated and observed O_3 mass concentrations are less than 50

μg m^{-3} in the plain area of BTH, and in several megacities, including Beijing, Tianjin, Baoding, and Shijiazhuang, the O_3 concentrations are less than 30 μg m^{-3} (Figure 6b). The low O_3 concentrations during the episode are generally caused by the weak insolation during wintertime, which is unfavorable for photochemical reactions, and the titration due to high NO_x emissions in BTH (Figure 6c). The simulated NO_2 concentrations are generally more than 40 μg m^{-3}, consistent with the observations at monitoring sites in BTH. The simulated and observed SO_2 mass concentrations in cities or their surrounding areas are still rather high, exceeding 50 μg m^{-3} (Figure 6d). Elevated SO_2 concentrations in BTH during wintertime are to some degree contributed by the residential coal combustion (Li et al., 2018). High levels of NO_2 and SO_2 show that stringent emission mitigation strategies still need to be implemented in BTH.

3.2.3 Sulfate, ammonium and SOA simulations in Beijing

The SOA and sulfate concentration directly influences the N_2O_5 heterogeneous hydrolysis in the Riemer09 parameterization, and the ammonium aerosol concentration substantially affects the nitrate aerosol formation. Therefore, Figure 7 presents the temporal profiles of observed and calculated SOA, sulfate, and ammonium mass concentrations at CRAES site in Beijing 10 to 27 February 2014. The model reasonably tracks the diurnal variation of the SOA concentration compared to observations, with the MB and IOA of -1.2 μg m^{-3} and 0.83, respectively. The observed SOA concentration exhibits rather large fluctuations, which is not well reproduced by the model. The simulated sulfate trend is generally in agreement with observations with an IOA of 0.88, but there are considerable model biases. During the first pollution event, the model reasonably reproduces the sulfate increase during the haze developing stage, but the early falloff of sulfate concentrations during the dissipation stage causes the substantial underestimation. However, during the second pollution event, the model considerably overestimates the sulfate concentration

against the measurement from 22 to 26 February 2014. The ammonium simulation is slightly better than that of sulfate, with an IOA of 0.90.

Furthermore, the MFB and MFE between simulations and observations are also calculated to evaluate the model performance in simulating meteorological parameters and air pollutants (Table 2). Boylan and Russell (2006) have proposed that MFB should be within ±60% and MFE should be below 75% for a satisfactory model performance. For the simulation in the B-case, MFB values are within 27% and MFE values are below 55%, indicating that the model performance is satisfactory.

In summary, the WRF-Chem model performs reasonably well in simulating air pollutants and aerosol species, showing that the simulated meteorological fields and emissions used in the study are generally reasonable.

3.3 Contributions of the N_2O_5 heterogeneous hydrolysis and organic coating to the nitrate formation

Figure 8 provides the nitrate temporal variations in the three cases against observations at CRAES site in Beijing from 10 to 27 February 2014. When the N_2O_5 heterogeneous hydrolysis is not considered in the H0-case, although the model well tracks the observed nitrate variations with an IOA of 0.91, it considerably underestimates nitrate concentration against the measurement, with a MB of -17.0 μg m^{-3}. When the N_2O_5 heterogeneous hydrolysis is taken into consideration based on the Riemer09 parameterization without organic coating in the C0-case, the nitrate simulation is improved compared to that in the H0-case, with an IOA of 0.95. However, the model commences to overestimate the nitrate concentration compared to the measurement, with a MB of 5.4 μg m^{-3}. In the B-case, when all the SOA is assumed to be involved in coating to suppress the N_2O_5 heterogeneous uptake on surfaces of deliquescent aerosols, the model performs best in simulating the nitrate variation compared to the measurement, with the MB and IOA of 0.1 μg m^{-3} and 0.96,

384 respectively. The remarkable consistency of the simulated nitrate in the B-case with the
385 measurement indicates that the organic coating plays an important role in improving the
386 nitrate simulation. It is worth noting that the MB for nitrate aerosols at CRAES site in the
387 B-case is close to zero, but the RMSE is still rather large, reaching 19.0 μg m^{-3}, showing
388 considerable underestimation and overestimation, caused by uncertainties of meteorological
389 fiends and emissions. For example, the model overestimates nitrate concentrations on 11, 13,
390 and 14 February and underestimation on 24 February against measurements. In addition, the
391 early occurrence of intensified winds in the morning on 16 February in simulations cause
392 rapid falloff of nitrate concentrations, leading to substantial model biases.

393 Figure 9a presents the distribution of contributions of the N_2O_5 heterogeneous
394 hydrolysis to the nitrate formation averaged during the episode by differentiating simulations
395 in the B-case and H0-case. The contribution of the N_2O_5 heterogeneous hydrolysis to the
396 nitrate formation is substantial in BTH, exceeding 15 μg m^{-3} in the plain area. Although the
397 O_3 concentration is fairly low in BTH during the episode (Figure 6b), particularly during
398 nighttime (Figure 5b), the elevated NO_2 level still facilitates the N_2O_5 formation to warrant
399 occurrence of the N_2O_5 heterogeneous hydrolysis. Previous studies have revealed that N_2O_5
400 heterogeneous hydrolysis is vital in nitrate formation. For example, Wang et al. (2017) have
401 calculated the daily average nitrate formation potential from the N_2O_5 heterogeneous
402 hydrolysis in Beijing, showing that the reaction accounts for 52% of the total nitrate
403 formation. Su et al. (2017) have investigated the contribution of N_2O_5 heterogeneous
404 hydrolysis to the nitrate formation in Beijing during autumn in 2015 and found that the
405 reaction causes a 21.0% enhancement of nitrate concentrations. In the present study, the
406 nitrate contribution of the N_2O_5 heterogeneous hydrolysis is 29.4% in Beijing during the
407 episode on average, which is close to the result in Su et al. (2017) but much lower than that in
408 Wang et al. (2017). The average nitrate contribution of the reaction in BTH is about 30.1%,

showing that the reaction constitutes an important nitrate source during the haze pollution episode. Additionally, the N_2O_5 heterogeneous hydrolysis contributes 11.6% of the $PM_{2.5}$ concentration on average, playing a considerable role in the haze formation in BTH.

However, it is worth noting that the brute force method (BFM) is used to quantify the contribution of the N_2O_5 heterogeneous hydrolysis to the nitrate formation (Dunker et al., 1996). The BFM is generally used to assess the importance of some source, but it lacks consideration of interactions of the complicated physical and chemical processes in the atmosphere (Zhang and Ying, 2011). Therefore, in the study, the contribution of the N_2O_5 heterogeneous hydrolysis to the nitrate formation might be underestimated, considering the competition of inorganic cations from HNO_3 formed through gas-phase reactions and sulfate aerosols in the atmosphere. It is imperative to use the source-oriented base module to evaluate the nitrate contribution of the reaction.

Figure 9b shows the distribution of the average decrease of nitrate concentrations due to suppression of organic coating during the episode by differentiating simulations in the B-case and C0-case. The organic coating reduces the nitrate concentration by more than 5 μg m^{-3} in the plain area of BTH, and on average, the decrease of nitrate aerosols is 4.7 μg m^{-3} or 8.4% in BTH during the episode. Riemer et al. (2009) have shown that when the nitrate levels are high (above 15 μg m^{-3}), the organic coating decreases nitrate concentrations by 10-15% over Europe. However, Cheng et al. (2018) have demonstrated that the suppression of organic coating is negligible over western and central Europe, with an influence on nitrate concentrations of less than 2% on average and 20% at the most significant moment. Apparently, except N_2O_5 and water soluble OA in the atmosphere, the effect of organic coating is also dependent on NH_3, RH, and temperature. Hence, the inconsistency between the model results about the organic coating effect can be attributed to the variation in simulation conditions. For example, in order to obtain substantial effects of the organic

coating, N_2O_5, SOA, and NH_3 need to be present when RH is high and temperature is low. However, those conditions are rarely fulfilled simultaneously over western and central Europe, causing a negligible effect of organic coating (Chen et al., 2018). Additionally, Wang et al. (2017) have indicated that the evaluated nitrate level with the N_2O_5 heterogeneous hydrolysis in Beijing is much higher than the observation, which they have attributed to atmospheric dilution and deposition. It is worth noting that the organic coating effect might constitute one of the most possible reasons for the overestimation of nitrate concentrations, considering the elevated SOA level in Beijing which suppresses the N_2O_5 heterogeneous hydrolysis and results in high observed N_2O_5 concentrations (Wu et al., 2017). Figure 10 presents the temporal variation of the simulated $\gamma_{N_2O_5}$ in Beijing during the episode. The simulated $\gamma_{N_2O_5}$ fluctuates between 0.009 and 0.02 when organic coating is included, with an average of 0.013. The estimated $\gamma_{N_2O_5}$ in Beijing by Wang et al. (2017) ranges from 0.025 to 0.072 without consideration of the suppression of organic coating, indicating that organic coating substantially hinders the N_2O_5 heterogeneous hydrolysis, likely causing the observed high level of N_2O_5 during nighttime.

It is worth noting that, in the study, the assumption of metastable aerosols is used or the water soluble aerosol is assumed to be only in liquid state in simulations. However, Wang et al. (2008) have highlighted the effect of the hysteresis of particle phase transitions on the distribution of solid and aqueous aerosols. The aerosol phase is generally regulated by the hysteresis loop. Atmospheric particles containing inorganic salts remain solid until the RH reaches the DRH (deliquescence relative humidity). At the DRH, the solid particle spontaneously absorbs water to become a saturated aqueous solution. However, the liquid particle does not crystallize when the RH is below the DRH (Seinfeld and Pandis, 2006). Therefore, another possible pathway exists to suppress the N_2O_5 hydrolysis, i.e., the inorganic particles might be in solid phase without organic coating. Further studies need to be

conducted to evaluate the hysteresis effect on the N_2O_5 hydrolysis and organic coating.

3.4 Sensitivity studies of organic aerosol hygroscopicity to the nitrate formation

In section 3.3, the WRF-Chem model considerably improves nitrate simulations when considering the N_2O_5 heterogeneous hydrolysis and organic coating effects. Organic aerosols (OA) are broadly classified as primary OA (POA) directly emitted and SOA formed in the atmosphere, some of which are water soluble. In order to explore the effects of different OA coating on the nitrate formation, additional four sensitivity studies are conducted, in which half of SOA (C1-case), all SOA (C2-case), all SOA and half of POA (C3-case), and all SOA and POA (C4-case) are involved in coating, respectively.

Figure 11 shows the Taylor diagram (Taylor, 2001) to present the variance, bias and correlation of the observed and simulated nitrate concentrations in the four sensitivity cases at CRAES site during the episode. In the C1-case, when half of SOA is considered to involve in coating, the simulated nitrate concentration is the best consistent with the observation, with a correlation coefficient of 0.96. In the C2-case with all SOA assumed to engage in coating, the correlation coefficient decreases to be 0.95. The normalized standardized deviation (NSD) is 1.02 for the C1-case and C2-case, showing the model overestimation in these two cases. With half of POA involved in coating, the NSD is very close to 1.0 (0.99), indicating the simulated nitrate concentration in the C3-case is almost the same as the observation on average, but the correlation coefficient of 0.94 is less than those in the C1-case and C2-case. When all of OA is assumed as the coating, the bias between simulated and observed nitrate concentrations is the largest, and the effect of POA on suppressing the N_2O_5 heterogeneous hydrolysis might be overestimated in the C4-case.

Sensitivity results show that the effects of different organic compounds on suppressing the N_2O_5 heterogeneous hydrolysis to form nitrate varies, depending on the content of water soluble OA. Laboratory and field measurements have revealed that OA becomes

progressively oxidized and more hygroscopic during the aging process in the atmosphere (Jimenez et al., 2009). The OA hygroscopicity constitutes a necessary prerequisite for accurately representing the organic coating effect on the N_2O_5 heterogeneous hydrolysis. According to the simulations in the present study, in BTH, not all of SOA can serve as the coating to suppress the nitrate formation, and the effect of POA on coating might be neglected. Xing et al. (2019) have shown that in BTH, the heterogeneous SOA formed by irreversible uptake of glyoxal and methylglyoxal on wet aerosol surfaces contributes about 30% of the SOA mass during haze days. Considering the possible heterogeneous SOA contribution of other carbonyl compounds and the atmospheric aging of OA, about half of SOA should likely be hygroscopic and involved in coating.

4 Conclusion

Nitrate aerosol has constituted a main component of $PM_{2.5}$ with implementation of aggressive emission control strategies since 2013 in BTH. In the study, the Riemer09 parameterization is implemented into the WRF-Chem model to simulate the nitrate formation from the N_2O_5 heterogeneous hydrolysis referred to as the most important pathway of the nitrate formation at nighttime. A heavy haze episode from 10 to 27 February 2014 in BTH is simulated using the WRF-Chem model to verify the effect of organic coating on the N_2O_5 heterogeneous hydrolysis and its consequent contribution to the nitrate formation. Analyses of synoptic fields show a stagnant weather condition with the prevailing southerly wind in the low-level atmosphere in BTH and surrounding areas during the episode, facilitating accumulation of air pollutants and heavy haze formation.

The WRF-Chem model performs reasonably in predicting the temporal variations of the meteorological parameters compared to observations in Beijing. The model generally reproduces well the temporal variations and spatial distributions of air pollutants against

observations at monitoring sites in BTH. In addition, the simulated diurnal profiles of sulfate, ammonium and SOA are also in good agreements with the measurements at CRAES site in Beijing.

The Riemer09 parameterization with all the SOA assumed to be involved in coating considerably improves the nitrate simulations compared to the measurements at CRAES site in Beijing. When organic coating is not considered in the Riemer09 parameterization, the model overestimates the nitrate concentration against the measurements. On average, organic coating decreases nitrate concentrations by 4.7 μg m^{-3} or 8.4% in BTH during the episode. Furthermore, the N_2O_5 heterogeneous hydrolysis with organic coating contributes about 30.1% of nitrate concentrations, and 11.6% of the $PM_{2.5}$ concentration in BTH, playing a considerable role in the haze formation.

Sensitivity studies reveal that the OA hygroscopicity is a necessary prerequisite for accurately evaluating the organic coating effect on the N_2O_5 heterogeneous hydrolysis. In the present study, POA might not serve as coating and about half of SOA should be involved in coating to suppress the nitrate formation. Future studies still need to be conducted to further predict the OA hygroscopicity, in order to more precisely represent the organic coating effect on the N_2O_5 heterogeneous hydrolysis in chemical transport models.

Author contribution. Guohui Li, as the contact author, provided the ideas and financial support, verified the conclusions, and revised the paper. Lang Liu conducted a research, designed the experiments, carried the methodology out, performed the simulation, processed the data, prepared the data visualization, and prepared the manuscript with contributions from all authors. Jiarui Wu and Xia Li provided the treatment of meteorological data, analyzed the study data, validated the model performance, and reviewed the manuscript. Suixin Liu, Yang

Qian, Tian Feng, and Jiamao Zhou provided the observation data used in the study, synthesized the observation, and reviewed the paper. Xuexi Tie and Junji Cao provided critical reviews pre-publication stage.

Acknowledgements. This work is financially supported by the National Key R&D Plan (Quantitative Relationship and Regulation Principle between Regional Oxidation Capacity of Atmospheric and Air Quality (2017YFC0210000)) and National Research Program for Key Issues in Air Pollution Control.

References

Aiken, A. C., DeCarlo, P. F., Kroll, J. H., Worsnop, D. R., Huff- man, J. A., Docherty, K. S., Ulbrich, I. M., Mohr, C., Kimmel, J. R., Sueper, D., Sun, Y., Zhang, Q., Trimborn, A., Northway, M., Ziemann, P. J., Canagaratna, M. R., Onasch, T. B., Alfarra, M. R., Prévôt, A. S. H., Dommen, J., Duplissy, J., Metzger, A., Baltensperger, U., and Jimenez, J. L.: O / C and OM / OC Ratios of Primary, Secondary, and Ambient Organic Aerosols with High- Resolution Time-of-Flight Aerosol Mass Spectrometry, Environ. Sci. Technol., 42, 4478–4485, https://doi.org/10.1021/es703009q, 2008.

Anttila, T., Kiendlerscharr, A., Tillmann, R., and Mentel, T. F.: On the reactive uptake of gaseous compounds by organic-coated aqueous aerosols: theoretical analysis and application to the heterogeneous hydrolysis of N_2O_5, J. Phys. Chem. A, 110, 10435–10443, https://doi.org/10.1021/jp062403c, 2006.

Bei, N., Wu, J., Elser, M., Feng, T., Cao, J., El-Haddad, I., Li, X., Huang, R., Li, Z., Long, X., Xing, L., Zhao, S., Tie, X., Prévôt, A. S. H., and Li, G.: Impacts of meteorological uncertainties on the haze formation in Beijing–Tianjin–Hebei (BTH) during wintertime: a case study, Atmos. Chem. Phys., 17, 14579–14591, https://doi.org/10.5194/acp-17-14579-2017, 2017.

Bertram, T. H. and Thornton, J. A.: Toward a general parameterization of N_2O_5 reactivity on aqueous particles: the competing effects of particle liquid water, nitrate and chloride, Atmos. Chem. and Phys., 9, 8351–8363, https://doi.org/10.5194/acp-9-8351-2009, 2009.

Binkowski, F. S. and Roselle, S. J.: Models-3 Community Multiscale Air Quality (CMAQ) model aerosol component 1. Model description, J. Geophys. Res.-Atmos., 108, 335–346, https://doi.org/10.1029/2001JD001409, 2003.

Boylan, J. W. and Russell, A. G.: PM and light extinction model performance metrics, goals, and criteria for three-dimensional air quality models, Atmos. Environ., 40, 4946–4959, https://doi.org/10.1016/j.atmosenv.2005.09.087, 2006.

Brown, S. S., Dubé, W. P., Tham, Y. J., Zha, Q., Xue, L., Poon, S., Wang, Z., Blake, D. R., Tsui, W., Parrish, D. D., and Wang, T.: Nighttime chemistry at a high altitude site above Hong Kong, J. Geophys. Res.-Atmos., 121, 2457–2475, https://doi.org/10.1002/2015JD024566, 2016.

Brown, S. S., Ryerson, T. B., Wollny, A. G., Brock, C. A., Peltier, R., Sullivan, A. P., Weber, R. J., Dubé, W. P., Trainer, M., and Meagher, J. F.: Variability in Nocturnal Nitrogen Oxide Processing and Its Role in Regional Air Quality, Science, 311, 67–70, https://doi.org/ 10.1126/science.1120120, 2006.

Cao, J. J., Lee, S. C., Ho, K. F., Zou, S. C., Fung, K., Li, Y., Watson, J. G., and Chow, J. C.: Spatial and seasonal variations of atmospheric organic carbon and elemental carbon in Pearl River Delta Region, China, Atmos. Environ., 38, 4447–4456, https://doi.org/10.1016/j.atmosenv.2004.05.016, 2004.

Cao, J. J., Lee, S. C., Chow, J. C., Watson, J. G., Ho, K. F., Zhang, R. J., Jin, Z. D., Shen, Z. X., Chen, G. C., Kang, Y. M., Zou, S. C., Zhang, L. Z., Qi, S. H., Dai, M. H., Cheng, Y., and Hu, K.: Spatial and seasonal distributions of carbonaceous aerosols over China, J. Geophys. Res.-Atmos., 112, D22S11, https://doi.org/10.1029/2006JD008205, 2007.

Chang, W. L., Bhave, P. V., Brown, S. S., Riemer, N., Stutz, J., and Dabdub, D.: Heterogeneous Atmospheric Chemistry, Ambient Measurements, and Model

592 Calculations of N_2O_5: A Review, Aerosol Sci. and Tech., 45, 665–695,
593 https://doi.org/10.1080/02786826.2010.551672, 2011.

594 Chen, F. and Dudhia, J.: Coupling an advanced land surface-hydrology model with the Penn
595 State-NCAR MM5 modeling system. Part I: Model implementation and sensitivity, Mon.
596 Weather Rev., 129, 569–585,
597 https://doi.org/10.1175/1520-0493(2001)129<0569:CAALSH>2.0.CO;2, 2001.

598 Chen, Y., Wolke, R., Ran, L., Birmili, W., Spindler, G., Schroder, W., Su, H., Cheng, Y.,
599 Tegen, I., and Wiedensoher, A.: A Parameterization of Heterogeneous Hydrolysis of
600 N_2O_5 for mass-based aerosol models: Improvement of Particulate Nitrate Prediction,
601 Atmos. Chem. and Phys., 8, 673–689, https://doi.org/10.5194/acp-18-673-2018, 2018.

602 Chou, M. D. and Suarez, M. J.: A solar radiation parameterization for atmospheric studies,
603 NASA TM-104606, Nasa Tech. memo 15, 1999.

604 Chou, M. D., Suarez, M. J., Liang, X. Z., Yan, M. H., and Cote, C.: A Thermal Infrared
605 Radiation Parameterization for Atmospheric Studies, NASA TM-2001-104606, Max J.,
606 19, 2001.

607 Davis, J. M., Bhave, P. V., and Foley, K. M.: Parameterization of N_2O_5 reaction probabilities
608 on the surface of particles containing ammonium, sulfate, and nitrate, Atmos. Chem. and
609 Phys., 8, 5295–5311, https://doi.org/10.5194/acp-8-5295-2008, 2008.

610 Dentener, F. J. and Crutzen, P. J.: Reaction of N_2O_5 on tropospheric aerosols: Impact on the
611 global distributions of NO_x, O_3, and OH, J. Geophys. Res.-Atmos., 98, 7149–7163,
612 https://doi.org/10.1029/92JD02979, 1993.

613 Dunker, A. M., Morris, R. E., Pollack, A. K., Schleyer, C. H., and Yarwood, G:
614 Photochemical modeling of the impact of fuels and vehicles on urban ozone using auto
615 oil program data, Environ. Sci. Technol., 30, 787–801,
616 https://doi.org/10.1021/es950175m, 1996.

617 Evans, M. J. and Jacob, D. J.: Impact of new laboratory studies of N_2O_5 hydrolysis on global
618 model budgets of tropospheric nitrogen oxides, ozone, and OH, Geophys. Res. Lett., 32,
619 297–314, https://doi.org/10.1029/2005GL022469, 2005.

620 Feng, T., Li, G., Cao, J., Bei, N., Shen, Z., Zhou, W., Liu, S., Zhang, T., Wang, Y., Huang,
621 R.-J., Tie, X., and Molina, L. T.: Simulations of organic aerosol concentrations during
622 springtime in the Guanzhong Basin, China, Atmos. Chem. Phys., 16, 10045–10061,
623 https://doi.org/10.5194/acp-16-10045-2016, 2016.

624 Fountoukis, C., Nenes, A., Sullivan, A., Weber, R., VanReken, T., Fischer, M., Matias, E.,
625 Moya, M. Farmer, D., and Cohen, R.: Thermodynamic characterization of Mexico City
626 Aerosol during MILAGRO 2006, Atmos. Chem. Phys., 9, 2141–2156, 2009.

627 Gao, M., Carmichael, G. R., Wang, Y., Saide, P. E., Yu, M., Xin, J., Liu, Z., and Wang, Z.:
628 Modeling study of the 2010 regional haze event in the North China Plain, Atmos. Chem.
629 Phys., 16, 1673–1691, https://doi.org/10.5194/acp-16-1673-2016, 2016.

630 Grell, G. A., Peckham, S. E., Schmitz, R., McKeen, S. A., Frost, G., Skamarock, W. C., and
631 Eder, B.: Fully coupled "online" chemistry within the WRF model, Atmos. Environ., 39,
632 6957–6975, 2005.

633 Guenther, A., Karl, T., Harley, P., Wiedinmyer, C., Palmer, P. I., and Geron, C.: Estimates of
634 global terrestrial isoprene emissions using MEGAN (Model of Emissions of Gases and

635 Aerosols from Nature), Atmos. Chem. and Phys., 6, 3181–3210,
636 https://doi.org/10.5194/acp-6-3181-2006, 2006.

637 Guo, S., Hu, M., Zamora, M. L., Peng, J., Shang, D., Zheng, J., Du, Z., Wu, Z., Shao, M., and
638 Zeng, L.: Elucidating severe urban haze formation in China, P. Natl. Acad. Sci. USA,
639 111, 17373–17378, https://doi.org/10.1073/pnas.1419604111, 2014.

640 Hess, P. G., Flocke, S., Lamarque, J. F., Barth, M. C., and Madronich, S.: Episodic modeling
641 of the chemical structure of the troposphere as revealed during the spring MLOPEX 2
642 intensive, J. Geophys. Res.-Atmos., 105, 26, 809–839, 2000.

643 Hong, S. Y. and Lim, J. O. J.: The WRF Single-Moment 6-Class Microphysics Scheme
644 (WSM6), Asia-Pacif. J. Atmos. Sci., 42, 129–151, 2006.

645 Horowitz, L. W., Walters, S., Mauzerall, D. L., Emmons, L. K., Rasch, P. J., Granier, C., Tie,
646 X., Lamarque, J. F., Schultz, M. G., Tyndall, G. S., Orlando, J. J., and Brasseur, G. P.: A
647 global simulation of tropospheric ozone and related tracers: Description and evaluation
648 of MOZART, version 2, J. Geophys. Res.-Atmos., 108, 4784,
649 https://doi.org/10.1029/2002JD002853, 2003.

650 Janjić, Z. I.: Nonsingular Implementation of the Mellor-Yamada Level 2.5 Scheme in the
651 NCEP Meso Model, NCEP Office Note 437, 2002.

652 Jimenez, J. L., Canagaratna, M. R., Donahue, N. M., Prevot, A. S. H., Zhang, Q., Kroll, J. H.,
653 DeCarlo, P. F., Allan, J. D., Coe, H., Ng, N. L., Aiken, A. C., Docherty, K. S., Ulbrich, I.
654 M., Grieshop, A. P., Robinson, A. L., Duplissy, J., Smith, J. D., Wilson, K. R., Lanz, V.
655 A., Hueglin, C., Sun, Y. L., Tian, J., Laaksonen, A., Raatikainen, T., Rautiainen, J.,
656 Vaattovaara, P., Ehn, M., Kulmala, M., Tomlinson, J. M., Collins, D. R., Cubison, M. J.,
657 Dunlea, E. J., Huffman, J. A., Onasch, T. B., Alfarra, M. R., Williams, P. I., Bower, K.,
658 Kondo, Y., Schneider, J., Drewnick, F., Borrnann, S., Weimer, S., Demerjian, K.,
659 Salcedo, D., Cottrell, L., Griffin, R., Takami, A., Miyoshi, T., Hatakeyama, S., Shimono,
660 A., Sun, J. Y., Zhang, M. Y., Dzepina, K., Kimmel, J. R., Sueper, D., Jayne, J. T.,
661 Herndon, S. C., Trimborn, A. M., Williams, L. R., Wood, E. C., Middlebrook, A. M.,
662 Kolb, C. E., Baltensperger, U., and Worsnop, D. R.: Evolution of organic aerosols in the
663 atmosphere, Science, 326(5959), 1525–1529, https://doi.org/ 10.1126/science.1180353,
664 2009.

665 Kim, Y. J., Spak, S. N., Carmichael, G. R., Riemer, N., and Stanier, C. O.: Modeled aerosol
666 nitrate formation pathways during wintertime in the Great Lakes region of North
667 America, J. Geophys. Res.-Atmos., 119, 12420–12445,
668 https://doi.org/10.1002/2014JD022320, 2014.

669 Li, G., Bei, N., Cao, J., Huang, R., Wu, J., Feng, T., Wang, Y., Liu, S., Zhang, Q., Tie, X.,
670 and Molina, L. T.: A possible pathway for rapid growth of sulfate during haze days in
671 China, Atmos. Chem. Phys., 17, 3301–3316, https://doi.org/10.5194/acp-17-3301-2017,
672 2017.

673 Li, G., Bei, N., Tie, X., and Molina, L. T.: Aerosol effects on the photochemistry in Mexico
674 City during MCMA-2006/MILAGRO campaign, Atmos. Chem. and Phys., 11, 5169–
675 5182, https://doi.org/10.5194/acp-11-5169-2011, 2011a.

676 Li, G., Lei, W., Bei, N., and Molina, L. T.: Contribution of garbage burning to chloride and
677 $PM_{2.5}$ in Mexico City, Atmos. Chem. and Phys. 12, 8751–8761,
678 https://doi.org/10.5194/acp-12-8751-2012, 2012.

679 Li, G., Lei, W., Zavala, M., Volkamer, R., Dusanter, S., Stevens, P., and Molina, L. T.:
680 Impacts of HONO sources on the photochemistry in Mexico City during the
681 MCMA-2006/MILAGO Campaign, Atmos. Chem. and Phys., 10, 6551–6567,
682 https://doi.org/10.5194/acp-10-6551-2010, 2010.

683 Li, G., Zavala, M., Lei, W., Tsimpidi, A. P., Karydis, V. A., Pandis, S. N., Canagaratna, M.
684 R., and Molina, L. T.: Simulations of organic aerosol concentrations in Mexico City
685 using the WRF-Chem model during the MCMA-2006/MILAGRO campaign, Atmos.
686 Chem. and Phys., 11, 3789–3809, https://doi.org/10.5194/acp-11-3789-2011, 2011b.

687 Li, G., Zhang, R., Fan, J., and Tie, X.: Impacts of black carbon aerosol on photolysis and
688 ozone, J. Geophys. Res.-Atmos., 110, D23206, https://doi.org/10.1029/2005JD005898,
689 2005.

690 Li, X., Wu, J., Elser, M., Feng, T., Cao, J., El-Haddad, I., Huang, R., Tie, X., Prévôt, A. S. H.,
691 and Li, G.: Contributions of residential coal combustion to the air quality in Beijing–
692 Tianjin–Hebei (BTH), China: a case study, Atmos. Chem. Phys., 18, 10675–10691,
693 https://doi.org/10.5194/acp-18-10675-2018, 2018.

694 Liggio, J., Li, S. M., and McLaren, R.: Reactive uptake of glyoxal by particulate matter, J.
695 Geophys. Res.-Atmos., 110, doi: 10.1029/2004jd005113, 2005.

696 Liu, W., Shen, G., Chen, Y., Shen, H., Huang, Y., Li, T., Wang, Y., Fu, X., Tao, S., Liu, W.,
697 Huang-Fu, Y., Zhang, W., Xue, C., Liu, G., Wu, F. and Wong, M.: Air pollution and
698 inhalation exposure to particulate matter of different sizes in rural households using
699 improved stoves in central China, J. Environ. Sci.-China, 63, 87–95,
700 doi:10.1016/j.jes.2017.06.019, 2018.

701 Lowe, D., Archer-Nicholls, S., Morgan, W., Allan, J., Utembe, S., Ouyang, B., Aruffo, E., Le
702 Breton, M., Zaveri, R. A., Di Carlo, P., Percival, C., Coe, H., Jones, R., and McFiggans,
703 G.: WRF-Chem model predictions of the regional impacts of N_2O_5 heterogeneous
704 processes on night-time chemistry over north-western Europe, Atmos. Chem. Phys., 15,
705 1385–1409, https://doi.org/10.5194/acp-15-1385-2015, 2015.

706 Nenes, A., Pandis, S. N., and Pilinis, C.: ISORROPIA: A new thermodynamic equilibrium
707 model for multiphase multicomponent inorganic aerosols, Aquat. Geochem., 4, 123–152,
708 https://doi.org/10.1023/a:1009604003981, 1998.

709 Riemer, N., Vogel, H., Vogel, B., Schell, B., Ackermann, I., Kessler, C., and Hass, H.:
710 Impact of the heterogeneous hydrolysis of N_2O_5 on chemistry and nitrate aerosol
711 formation in the lower troposphere under photosmog conditions, J. Geophys.
712 Res.-Atmos., D4, 4144, https://doi.org/10.1029/2002JD002436, 2003.

713 Riemer, N., Vogel, H., Vogel, B., Anttila, T., Kiendler-Scharr, A., and Mentel, T.F.: Relative
714 importance of organic coatings for the heterogeneous hydrolysis of N_2O_5 during summer
715 in Europe, J. Geophys. Res.-Atmos., D17307, https://doi.org/10.1029/2008JD011369,
716 2009.

717 Robinson, A. L., Donahue, N. M., Shrivastava, M. K.,Weitkamp, E. A., Sage, A. M.,
718 Grieshop, A. P., Lane, T. E., Pandis, S. N., and Pierce, J. R.: Rethinking organic aerosols:
719 semivolatile emissions and photochemical aging, Science, 315, 1259–1262, 2007.

720 Seinfeld, J. H. and Pandis, S. N.: Atmospheric Chemistry and Physics: From Air Pollution to
721 Climate Change, 2nd Edn., John Wiley & Sons Inc., New York, 2006.

Shrivastava, M. K., Lane, T. E., Donahue, N. M., Pandis, S. N., and Robinson, A. L.: Effects of gas particle partitioning and aging of primary emissions on urban and regional organic aerosol concentrations, J. Geophys. Res.-Atmos., 113, doi: 10.1029/2007jd009735, 2008.

Strader, R.: Evaluation of secondary organic aerosol formation in winter, Atmos. Environ., 33, 4849–4863, https://doi.org/10.1016/s1352- 2310(99)00310-6, 1999.

Sun, Y. L., Wang, Z. F., Fu, P. Q., Yang, T., Jiang, Q., Dong, H. B., Li, J., and Jia, J. J.: Aerosol composition, sources and processes during wintertime in Beijing, China, Atmos. Chem. Phys., 13, 4577–4592, https://doi.org/10.5194/acp-13-4577-2013, 2013.

Sun, Y. L., Wang, Z. F., Du, W., Zhang, Q., Wang, Q. Q., Fu, P. Q., Pan, X. L., Li, J., Jayne, J., and Worsnop, D. R.: Long-term real-time measurements of aerosol particle composition in Beijing, China: seasonal variations, meteorological effects, and source analysis, Atmos. Chem. Phys., 15, 10149–10165, https://doi.org/10.5194/acp-15-10149-2015, 2015.

Tao, J., Zhang, L., Cao, J., and Zhang, R.: A review of current knowledge concerning $PM_{2.5}$ chemical composition, aerosol optical properties and their relationships across China, Atmos. Chem. Phys., 17, 9485–9518, https://doi.org/10.5194/acp-17-9485-2017, 2017.

Taylor, K. E.: Summarizing multiple aspects of model performance in a single diagram, J. Geophys. Res.-Atmos., 106(D7), 7183–7192, https://doi.org/10.1029/2000JD900719, 2001.

Tie, X., Madronich, S., Walters, S., Zhang, R., Rasch, P., and Collins, W.: Effect of clouds on photolysis and oxidants in the troposphere, J. Geophys. Res.-Atmos., 108, 4642, https://doi.org/10.1029/2003JD003659, 2003.

Volkamer, R., Martini, F. S., Molina, L. T., Salcedo, D., Jimenez, J. L., and Molina, M. J.: A missing sink for gas-phase glyoxal in Mexico City: Formation of secondary organic aerosol, Geophys. Res. Lett., 34, doi: 10.1029/2007gl030752, 2007.

Wang, G., Zhang, R., Gomez, M. E., Yang, L., Levy Zamora, M., Hu, M., Lin, Y., Peng, J., Guo, S., Meng, J., Li, J., Cheng, C., Hu, T., Ren, Y., Wang, Y., Gao, J., Cao, J., An, Z., Zhou, W., Li, G., Wang, J., Tian, P., Marrero-Ortiz, W., Secrest, J., Du, Z., Zheng, J., Shang, D., Zeng, L., Shao, M., Wang, W., Huang, Y., Wang, Y., Zhu, Y., Li, Y., Hu, J., Pan, B., Cai, L., Cheng, Y., Ji, Y., Zhang, F., Rosenfeld, D., Liss, P. S., Duce, R. A., Kolb, C. E., and Molina, M. J.: Persistent sulfate formation from London Fog to Chinese haze, P. Natl. Acad. Sci. USA, 113(48), 13630–13635, https://doi.org/10.1073/pnas.1616540113, 2016.

Wang, H., Lu, K., Chen, X., Zhu, Q., Chen, Q., Guo, S., Jiang, M., Li, X., Shang, D., Tan, Z., Wu, Y., Wu, Z., Zou, Q., Zheng, Y., Zeng, L., Zhu, T., Hu, M., and Zhang, Y.: High N_2O_5 concentrations observed in urban Beijing: Implications of a large nitrate formation Pathway, Environ. Sci. Tech. Lett., 4, 416–420, https://doi.org/10.1021/acs.estlett.7b00341, 2017.

Wang, J., Hoffmann, A. A., Park, R. J., Jacob, D. J., and Martin, S. T.: Global distribution of solid and aqueous sulfate aerosols: Effect of the hysteresis of particle phase transitions, J. Geophys. Res.-Atmos., 113, D11206, https://doi.org/10.1029/2007JD009367, 2008.

Wei, S., Shen, G., Zhang, Y., Xue, M., Xie, H., Lin, P., Chen, Y., Wang, X. and Tao, S.:

766 Field measurement on the emissions of PM, OC, EC and PAHs from indoor crop straw
767 burning in rural China, Environ. Pollut., 184, 18–24, doi:10.1016/j.envpol.2013.07.036,
768 2014.

769 Wesely, M. L.: Parameterization of surface resistances to gaseous dry deposition in
770 regional-scale numerical models, Atmos. Environ., 23, 1293–1304,
771 https://doi.org/10.1016/0004-6981(89)90153-4, 1989.

772 Wu, J., Li, G., Cao, J., Bei, N., Wang, Y., Feng, T., Huang, R., Liu, S., Zhang, Q., and Tie, X.:
773 Contributions of trans-boundary transport to summertime air quality in Beijing, China,
774 Atmos. Chem. Phys., 17, 2035–2051, https://doi.org/10.5194/acp-17-2035-2017, 2017.

775 Xing, L., Wu, J., Elser, M., Tong, S., Liu, S., Li, X., Liu, L., Cao, J., Zhou, J., El-Haddad, I.,
776 Huang, R., Ge, M., Tie, X., Prévôt, A. S. H., and Li, G.: Wintertime secondary organic
777 aerosol formation in Beijing–Tianjin–Hebei (BTH): contributions of HONO sources and
778 heterogeneous reactions, Atmos. Chem. Phys., 19, 2343–2359,
779 https://doi.org/10.5194/acp-19-2343-2019, 2019.

780 Yu, X. Y., Cary, R. A., and Laulainen, N. S.: Primary and secondary organic carbon
781 downwind of Mexico City, Atmos. Chem. Phys., 9, 6793–6814,
782 https://doi.org/10.5194/acp-9-6793-2009, 2009.

783 Zhang, H. and Ying, Q.: Secondary organic aerosol formation and source apportionment in
784 Southeast Texas, Atmos. Environ., 45: 3217–3227,
785 https://doi.org/10.1016/j.atmosenv.2011.03.046, 2011.

786 Zhang, Q., Streets, D. G., Carmichael, G. R., He, K., Huo, H., Kannari, A., Klimont, Z., Park,
787 I. S., Reddy, S., Fu, J., Chen, D., Duan, L., Lei, Y.,Wang, L., and Yao, Z.: Asian
788 emissions in 2006 for the NASA INTEX-B mission, Atmos. Chem. and Phys., 9, 5131–
789 5153, https://doi.org/10.5194/acp-9-5131-2009, 2009.

790 Zhang, R., Jing, J., Tao, J., Hsu, S., Wang, G., Cao, J., Lee, C., Zhu, L., Chen, Z., and Zhao,
791 Y.: Chemical characterization and source apportionment of $PM_{2.5}$ in Beijing: seasonal
792 perspective, Atmos. Chem. and Phys., 13, 7053–7074,
793 https://doi.org/10.5194/acp-13-7053-2013, 2013.

794 Zhang, X. Y., Wang, J. Z., Wang, Y. Q., Liu, H. L., Sun, J. Y., and Zhang, Y. M.: Changes in
795 chemical components of aerosol particles in different haze regions in China from 2006
796 to 2013 and contribution of meteorological factors, Atmos. Chem. and Phys., 15, 19197–
797 19238, https://doi.org/ 10.5194/acp-15-12935-2015, 2015.

798 Zhang, X. Y., Wang, Y. Q., Niu, T., Zhang, X. C., Gong, S. L., Zhang, Y. M., and Sun, J. Y.:
799 Atmospheric aerosol compositions in China: spatial/temporal variability, chemical
800 signature, regional haze distribution and comparisons with global aerosols, Atmos.
801 Chem. and Phys., 12, 779–799, https://doi.org/10.5194/acp-12-779-2012, 2012.

802 Zhao, J., Levitt, N. P., Zhang, R., and Chen, J.: Heterogeneous reactions of methylglyoxal in
803 acidic media: Implications for secondary organic aerosol formation, Environ. Sci.
804 Technol., 40, 7682–7687, doi: 10.1021/es060610k, 2006.

805 Zhao, P. S., Dong, F., He, D., Zhao, X. J., Zhang, X. L., Zhang, W. Z., Yao, Q., and Liu, H.
806 Y.: Characteristics of concentrations and chemical compositions for $PM_{2.5}$ in the region
807 of Beijing, Tianjin, and Hebei, China, Atmos. Chem. and Phys., 13, 4631–4644,
808 https://doi.org/10.5194/acp-13-4631-2013, 2013.

809 Zheng, B., Zhang, Q., Zhang, Y., He, K. B., Wang, K., Zheng, G. J., Duan, F. K., and Ma, Y.
810 L., Kimoto, T.: Heterogeneous chemistry: a mechanism missing in current models to
811 explain secondary inorganic aerosol formation during the January 2013 haze episode in
812 North China, Atmos. Chem. and Phys., 2031–2049,
813 https://doi.org/10.5194/acp-15-2031-2015, 2015.

814

815

816

817

818

819 **Table 1** WRF-Chem model configurations.

820

Regions	Beijing-Tianjin-Hebei (BTH)
Simulation period	February 10 to 27, 2014
Domain size	200 × 200
Domain center	38.0°N, 116.0°E
Horizontal resolution	6km × 6km
Vertical resolution	35 vertical levels with a stretched vertical grid with spacing ranging from 30m near the surface, to 500m at 2.5km and 1km above 14km
Microphysics scheme	WSM 6-class graupel scheme (Hong and Lim, 2006)
Boundary layer scheme	MYJ TKE scheme (Janjić, 2002)
Surface layer scheme	MYJ surface scheme (Janjić, 2002)
Land-surface scheme	Unified Noah land-surface model (Chen and Dudhia, 2001)
Long-wave radiation scheme	Goddard longwave scheme (Chou and Suarez, 2001)
Short-wave radiation scheme	Goddard shortwave scheme (Chou and Suarez, 1999)
Meteorological boundary and initial conditions	NCEP 1°×1° reanalysis data
Chemical initial and boundary conditions	MOZART 6-hour output (Horowitz et al., 2003)
Anthropogenic emission inventory	SAPRC-99 chemical mechanism emissions (Zhang et al., 2009)
Biogenic emission inventory	MEGAN model developed by Guenther et al. (2006)
Model spin-up time	24 hours

821

822

823

824

825

Table 2 Statistics for model performance.

	MFB (%)	MFE (%)	MB	RMSE	IOA
[a]Temperature	-3.7	8.5	-0.2 ˚C	1.7 ˚C	0.94
[a]Relative humidity	5.2	15.7	2.6 %	10.9 %	0.89
[a]Wind speed	16.3	38.6	0.3 m s^{-1}	1.0 m s^{-1}	0.73
[a]Wind direction	26.3	54.6	21.9 ˚	90.4 ˚	0.66
[b]$PM_{2.5}$	-3.0	13.5	-6.3 μg m^{-3}	27.6 μg m^{-3}	0.96
[b]O_3	2.1	28.3	1.4 μg m^{-3}	10.3 μg m^{-3}	0.91
[b]NO_2	10.6	16.2	6.6 μg m^{-3}	13.0 μg m^{-3}	0.92
[b]SO_2	6.1	23.9	7.6 μg m^{-3}	27.8 μg m^{-3}	0.85
[b]CO	10.6	18.5	0.2 mg m^{-3}	0.5 mg m^{-3}	0.90
[c]SOA	-14.5	52.9	-1.2 μg m^{-3}	15.5 μg m^{-3}	0.83
[c]Sulfate	23.8	53.0	4.5 μg m^{-3}	26.5 μg m^{-3}	0.88
[c]Ammonium	22.2	44.2	2.9 μg m^{-3}	16.4 μg m^{-3}	0.90
[c]Nitrate	7.1	37.1	0.1 μg m^{-3}	19.0 μg m^{-3}	0.96

a, b, and c represent the meteorological parameter averaged over 12 meteorological sites in Beijing, the air pollutant averaged over all ambient monitoring stations in BTH, and the aerosol component at the CRAES site in Beijing, respectively.

Figure Captions

Figure 1 WRF-Chem simulation domain with topography. The red filled circles show the locations of the cities with ambient air quality monitoring sites, and the size of the circles represents the number of sites in each city. The blue filled rectangle denotes the CRAES observation site in Beijing.

Figure 2 Distributions of average winds (black flag vectors), geopotential heights (blue lines), temperature (red lines), and relative humidity (contour fill) at (a) and (b) 500hPa and (c) and (d) 850hPafrom 10 to 27 February 2014, respectively.

Figure 3 Temporal variations of simulated (red line) and observed (black dots) meteorological parameters of near-surface (a) temperature, (b) relative humidity, (c) wind speed, and (d) wind direction averaged at 12 meteorological sites in Beijing from 10 to 27 February 2014.

Figure 4 Relationships between observed and simulated mass concentrations of $PM_{2.5}$, O_3, NO_2, SO_2, and CO in Beijing, Tianjin, and Hebei from 10 to 27 February 2014. The red line is the linear regression between observations and simulations, and the black dashed line presents the 1:1 line.

Figure 5 Comparison of observed (black dots) and simulated (red line) diurnal profiles of near surface hourly (a) $PM_{2.5}$, (b) O_3, (c) NO_2, (d) SO_2, and (e) CO averaged over all ambient monitoring stations in BTH from 10 to 27 February 2014.

Figure 6 Spatial distributions of average (a) $PM_{2.5}$, (b) O_3, (c) NO_2, and (d) SO_2 mass concentrations from 10 to 27 February 2014. Colored dots, colored contour, and black arrows are observations, simulations, and simulated surface winds, respectively.

Figure 7 Comparison of observed (black dots) and simulated (red line) diurnal profiles of hourly (a) SOA, (b) sulfate, and (c) ammonium concentrations at CRAES site in Beijing from 10 to 27 February 2014.

Figure 8 Temporal variations of observed (black dot) and the simulated (Green line: H0-case; Blue line: C0-case; Red line: B-case) nitrate concentrations at CRAES site in Beijing from 10 to 27 February 2014.

Figure 9 Spatial distributions of average nitrate contributions of (a) the N_2O_5 heterogeneous hydrolysis and (b) organic coating in BTH from 10 to 27 February 2014.

Figure 10 Temporal variation of the simulated $\gamma_{N_2O_5}$ in the B-case in Beijing from 10 to 27 February 2014.

Figure 11 Taylor diagram (Taylor, 2001) to present the variance, bias and correlation of the observed and simulated nitrate concentrations at CRAES site in Beijing from 10 to 27 February 2014.

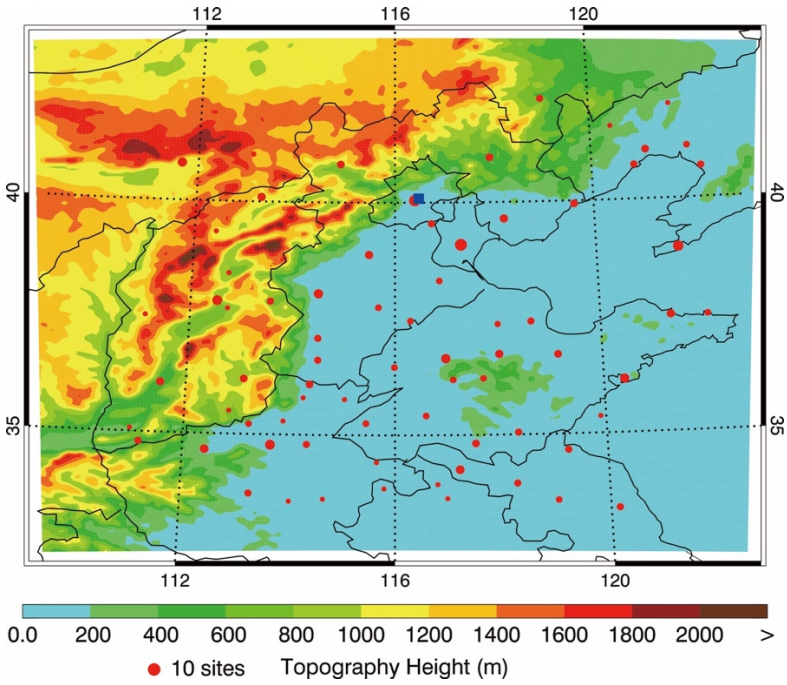

Figure 1 WRF-Chem simulation domain with topography. The red filled circles show the locations of the cities with ambient air quality monitoring sites, and the size of the circles represents the number of sites in each city. The blue filled rectangle denotes the CRAES observation site in Beijing.

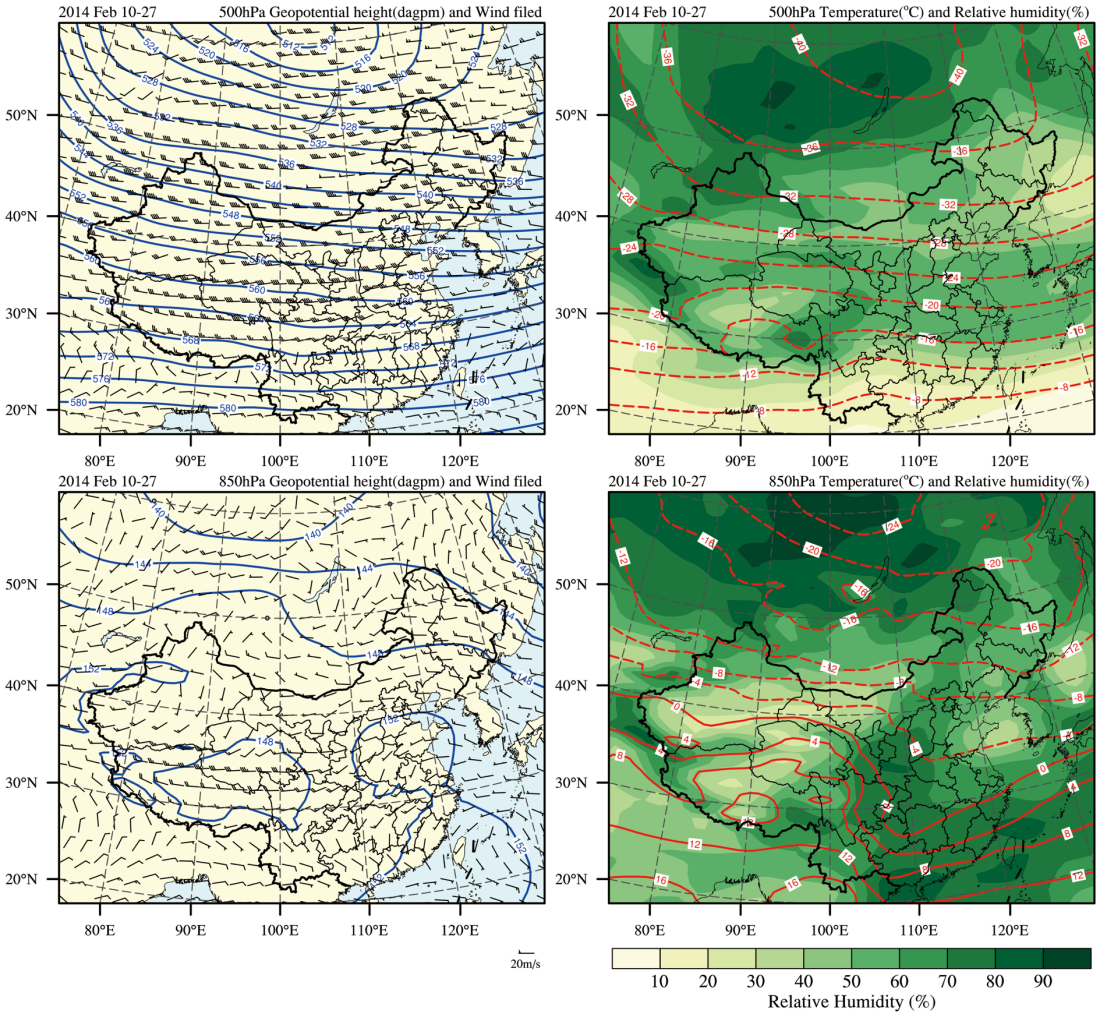

Figure 2 Distributions of average winds (black flag vectors), geopotential heights (blue lines), temperature (red lines), and relative humidity (contour fill) at (a) and (b) 500hPa and (c) and (d) 850hPafrom 10 to 27 February 2014, respectively.

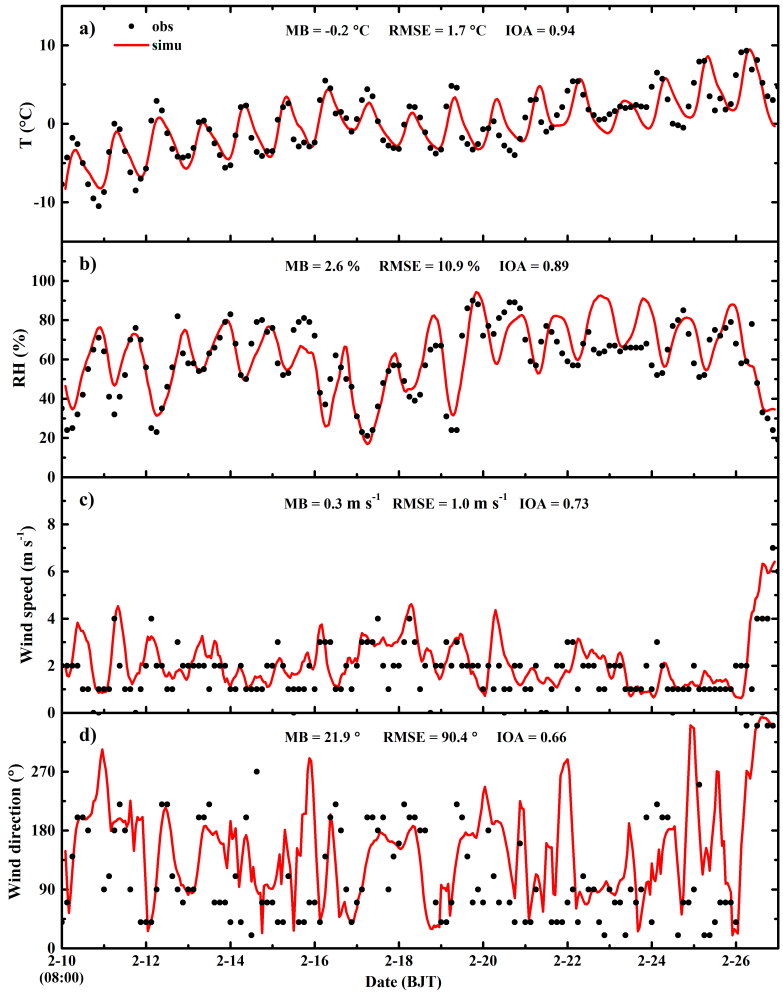

Figure 3 Temporal variations of simulated (red line) and observed (black dots) meteorological parameters of near-surface (a) temperature, (b) relative humidity, (c) wind speed, and (d) wind direction averaged at 12 meteorological sites in Beijing from 10 to 27 February 2014.

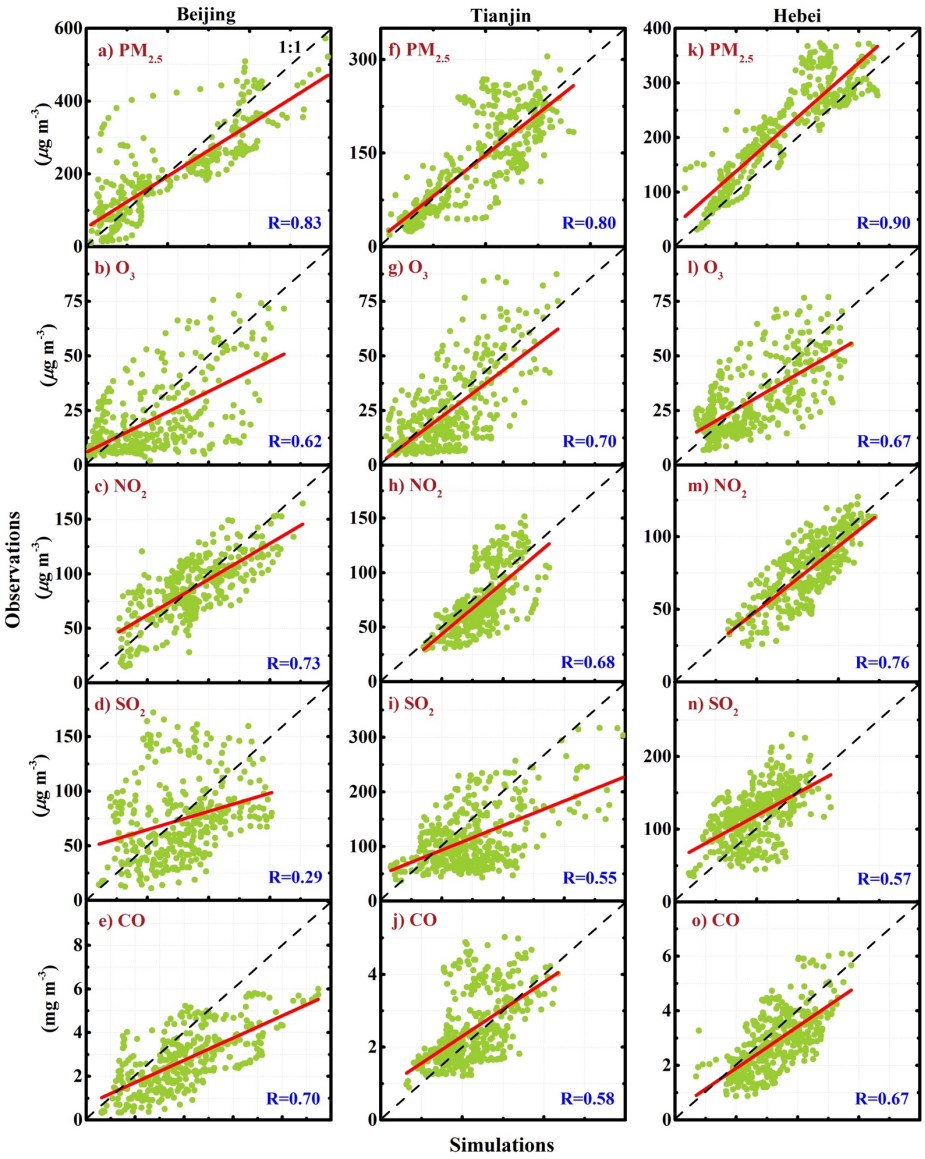

Figure 4 Relationships between observed and simulated mass concentrations of $PM_{2.5}$, O_3, NO_2, SO_2, and CO in Beijing, Tianjin, and Hebei from 10 to 27 February 2014. The red line is the linear regression between observations and simulations, and the black dashed line presents the 1:1 line.

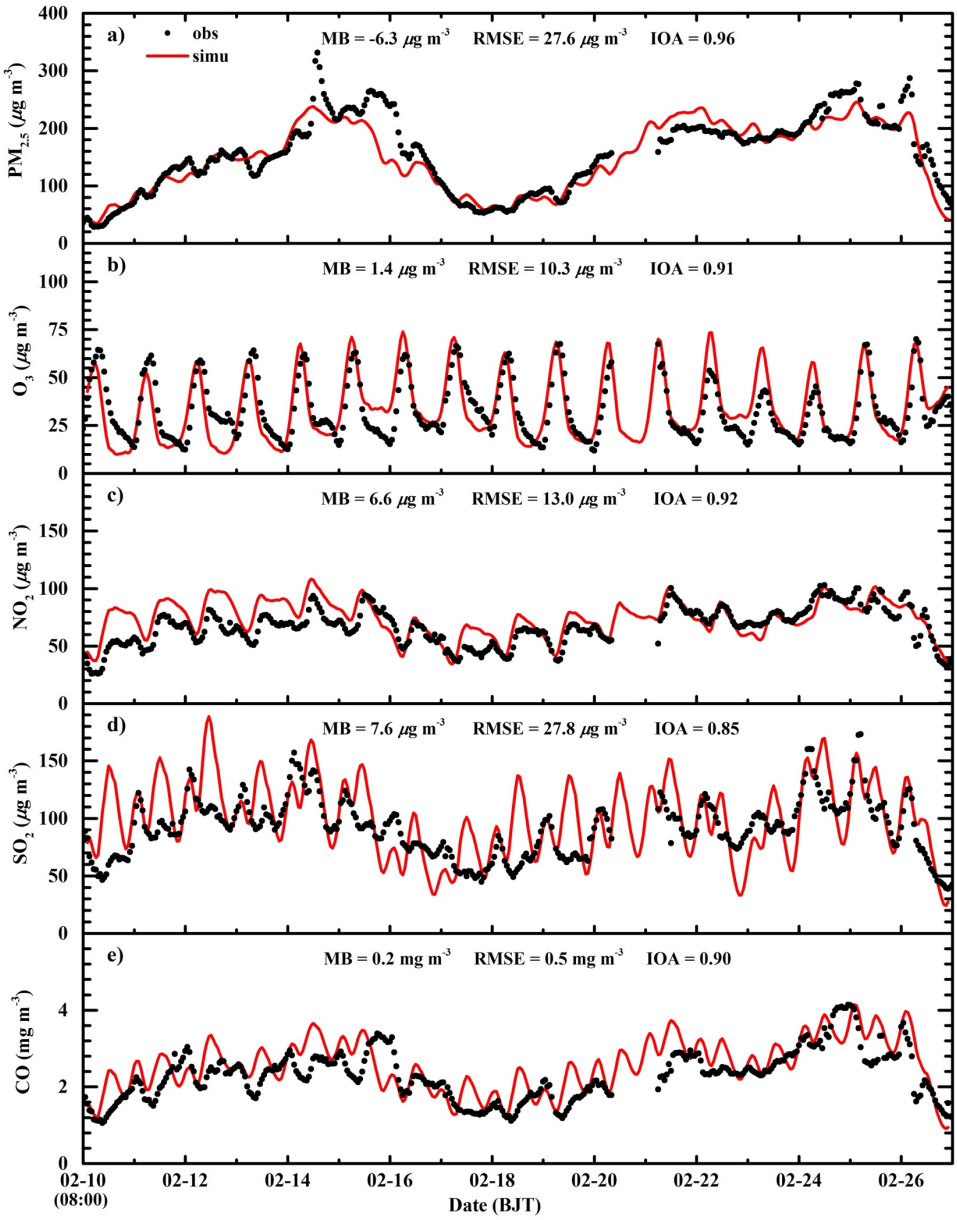

Figure 5 Comparison of observed (black dots) and simulated (red line) diurnal profiles of near surface hourly (a) $PM_{2.5}$, (b) O_3, (c) NO_2, (d) SO_2, and (e) CO averaged over all ambient monitoring stations in BTH from 10 to 27 February 2014.

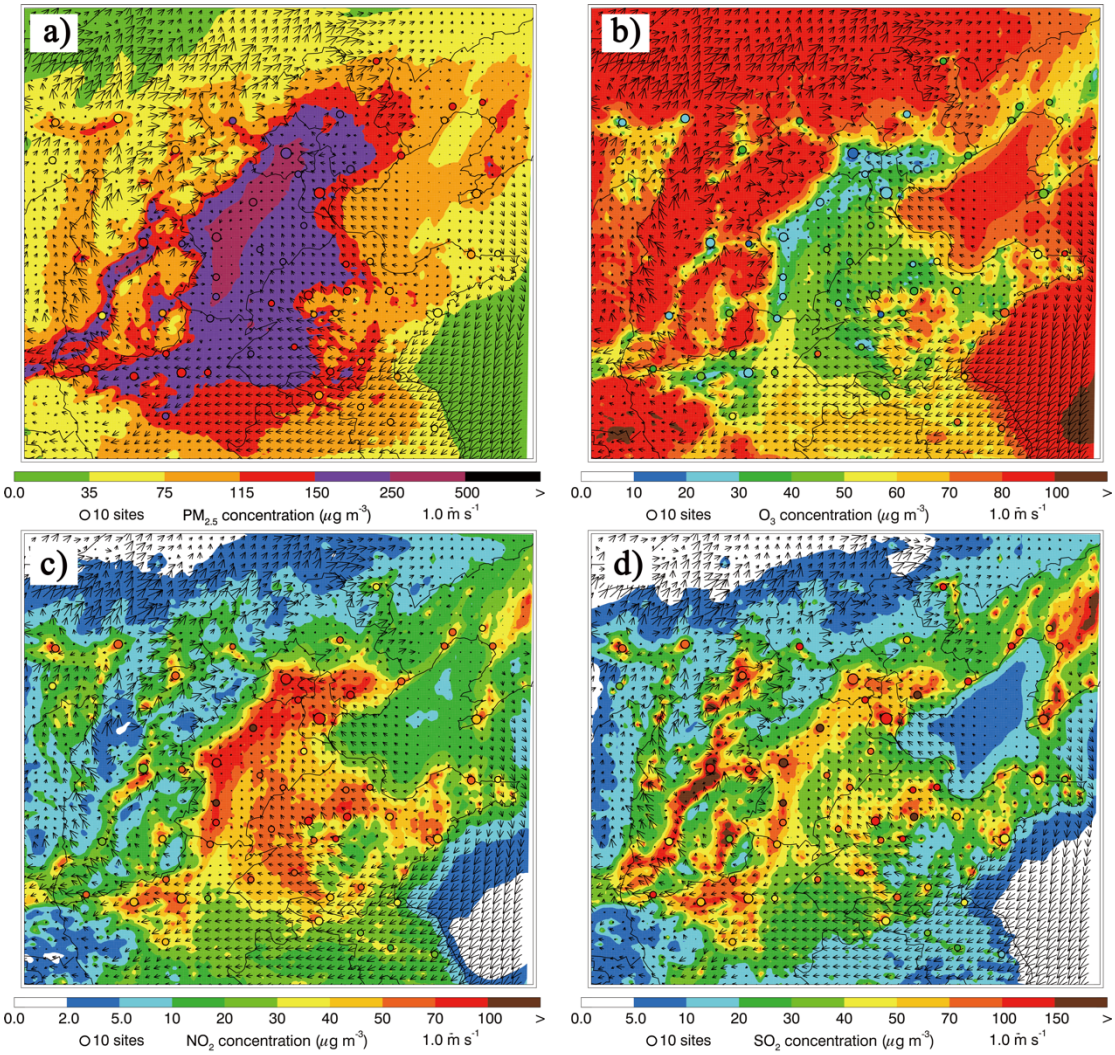

Figure 6 Spatial distributions of average (a) $PM_{2.5}$, (b) O_3, (c) NO_2, and (d) SO_2 mass concentrations from 10 to 27 February 2014. Colored dots, colored contour, and black arrows are observations, simulations, and simulated surface winds, respectively.

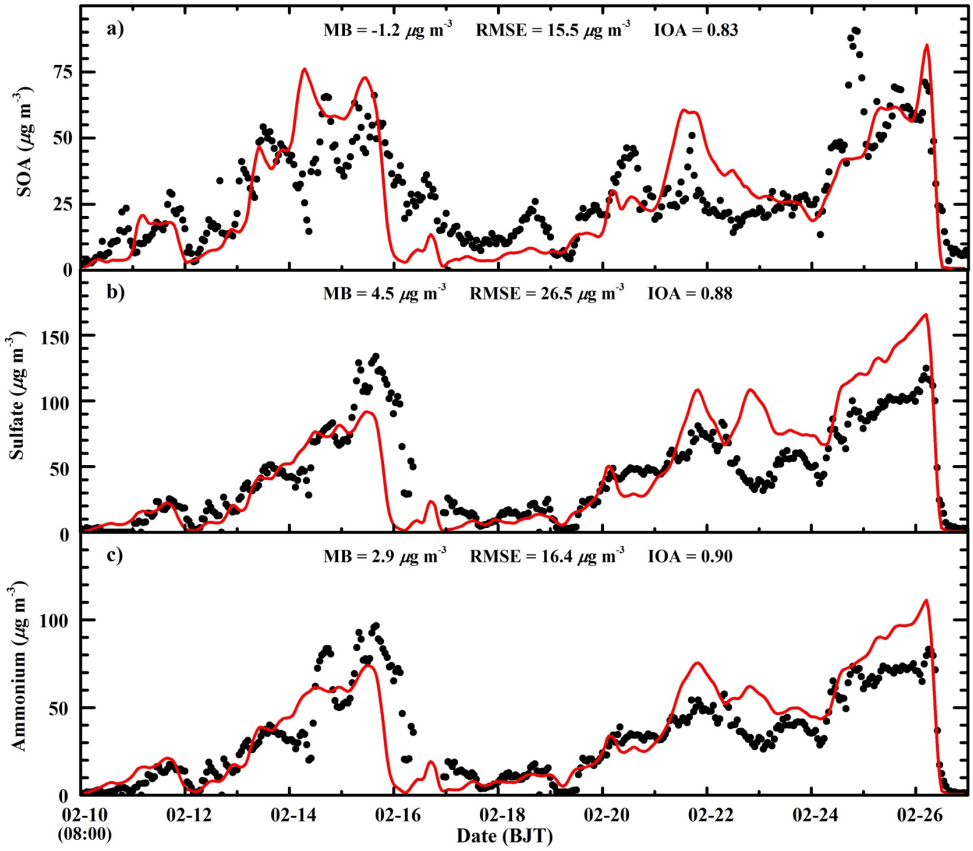

Figure 7 Comparison of observed (black dots) and simulated (red line) diurnal profiles of hourly (a) SOA, (b) sulfate, and (c) ammonium concentrations at CRAES site in Beijing from 10 to 27 February 2014.

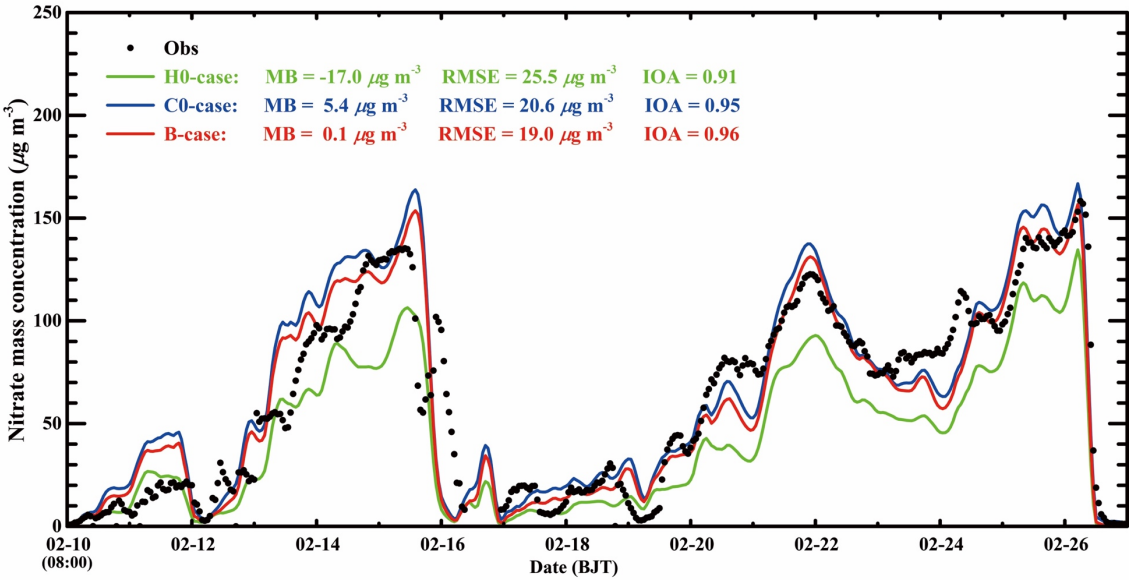

Figure 8 Temporal variations of observed (black dot) and the simulated (Green line: H0-case; Blue line: C0-case; Red line: B-case) nitrate concentrations at CRAES site in Beijing from 10 to 27 February 2014.

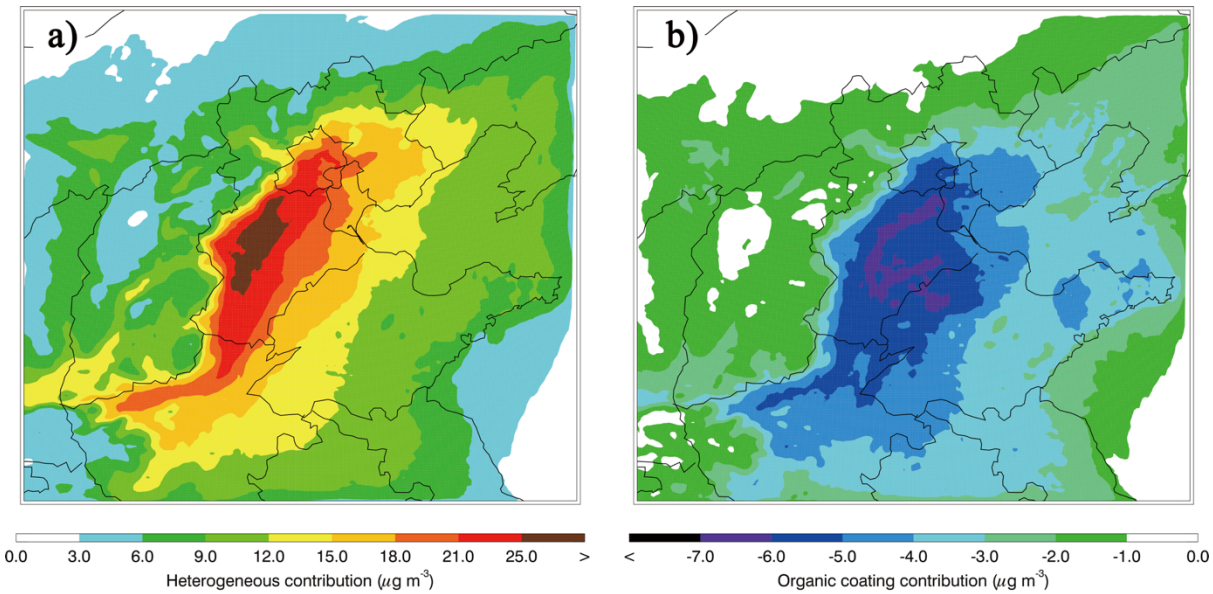

Figure 9 Spatial distributions of average nitrate contributions of (a) the N_2O_5 heterogeneous hydrolysis and (b) organic coating in BTH from 10 to 27 February 2014.

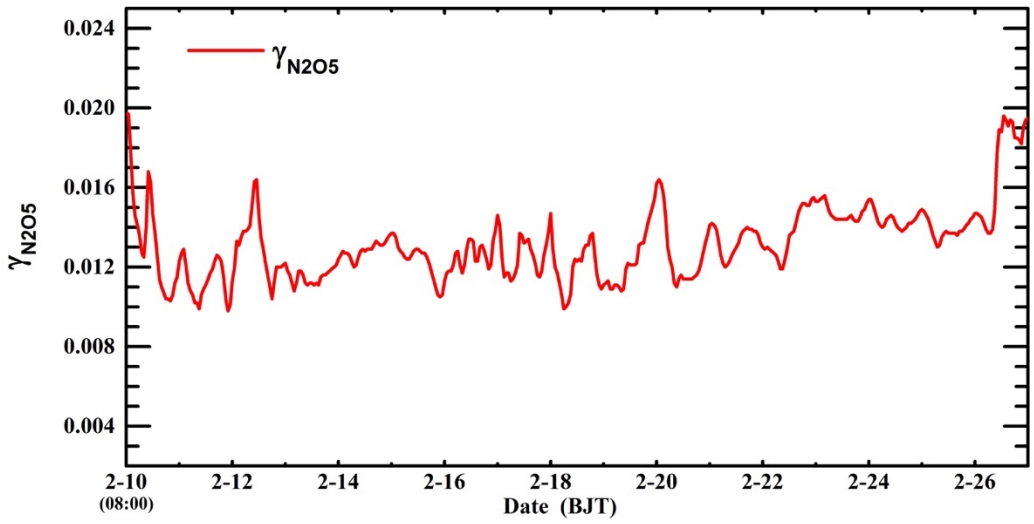

Figure 10 Temporal variation of the simulated $\gamma_{N_2O_5}$ in the B-case in Beijing from 10 to 27 February 2014.

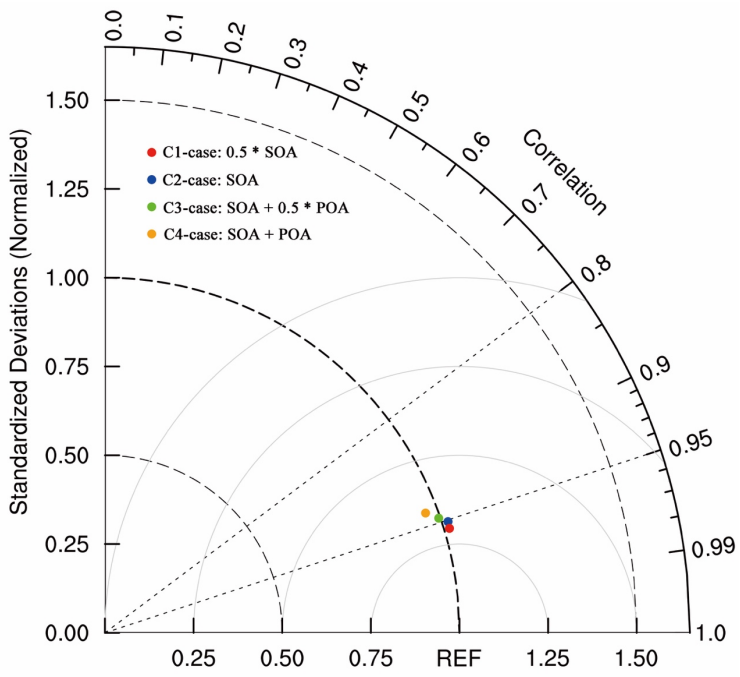

977
978
979 Figure 11 Taylor diagram (Taylor, 2001) to present the variance, bias and correlation of the
980 observed and simulated nitrate concentrations at CRAES site in Beijing from 10 to 27
981 February 2014.
982
983
984
985